A series of nickel(II) thiocyanate complexes comprising various molar contents of isonicotinamide and water as ligands or co-crystallized moieties – An experimental and theoretical study

Lucija Hok,[a] Robert Vianello,*[a] Dubravka Matković-Čalogović[b], Ljiljana Karanović,[c] Sunčica Roca,[a] Jarosław Jaźwiński,[d] Marina Tašner,[b] Darko Vušak,[b] Marijana Đaković,[b] and Zora Popović*[b]

SUPPORTING INFORMATION

Contents

Table S1.1. Crystallization screening conditions. Volumes of stock solutions used for screening (*V* = 100 µL; stock solutions: 1M nickel nitrate. 2M KSCN. 0.5 M isonicotinamide).

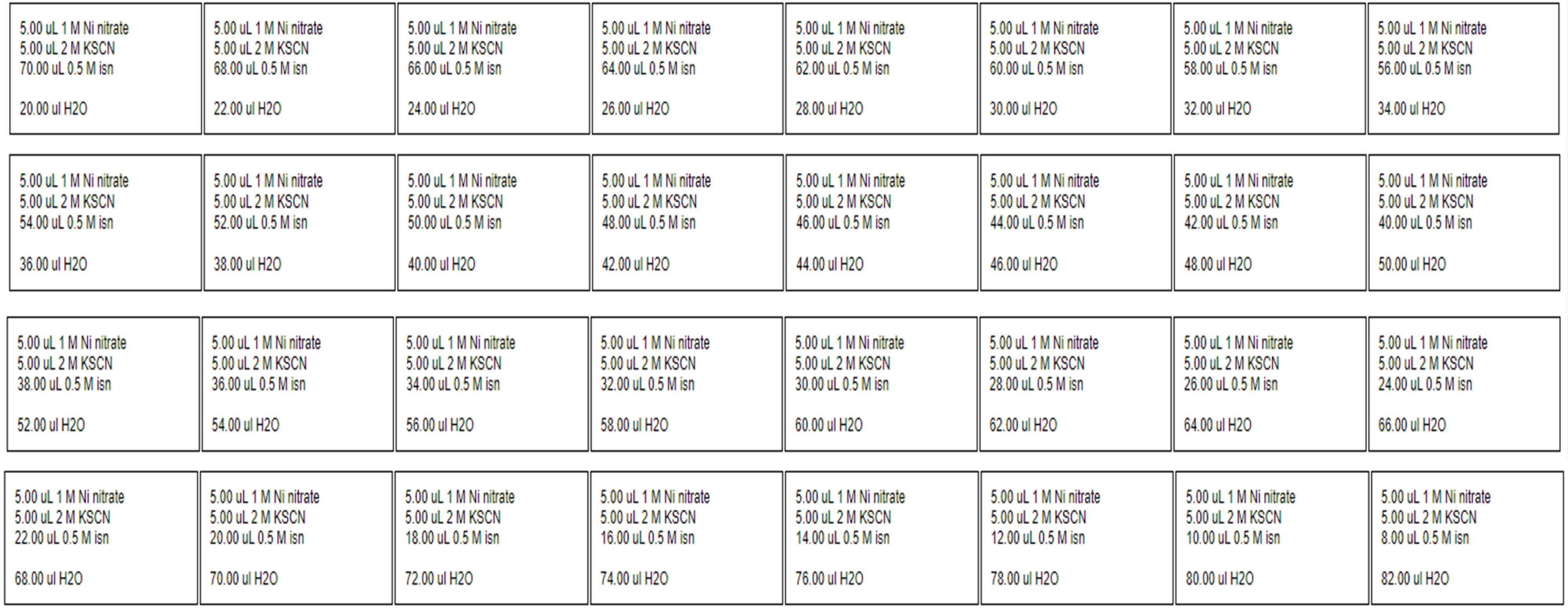

	1	2	3	4	5	6	7	8
A	5.00 uL 1 M Ni nitrate 5.00 uL 2 M KSCN 70.00 uL 0.5 M isn 20.00 ul H2O	5.00 uL 1 M Ni nitrate 5.00 uL 2 M KSCN 68.00 uL 0.5 M isn 22.00 ul H2O	5.00 uL 1 M Ni nitrate 5.00 uL 2 M KSCN 66.00 uL 0.5 M isn 24.00 ul H2O	5.00 uL 1 M Ni nitrate 5.00 uL 2 M KSCN 64.00 uL 0.5 M isn 26.00 ul H2O	5.00 uL 1 M Ni nitrate 5.00 uL 2 M KSCN 62.00 uL 0.5 M isn 28.00 ul H2O	5.00 uL 1 M Ni nitrate 5.00 uL 2 M KSCN 60.00 uL 0.5 M isn 30.00 ul H2O	5.00 uL 1 M Ni nitrate 5.00 uL 2 M KSCN 58.00 uL 0.5 M isn 32.00 ul H2O	5.00 uL 1 M Ni nitrate 5.00 uL 2 M KSCN 56.00 uL 0.5 M isn 34.00 ul H2O
B	5.00 uL 1 M Ni nitrate 5.00 uL 2 M KSCN 54.00 uL 0.5 M isn 36.00 ul H2O	5.00 uL 1 M Ni nitrate 5.00 uL 2 M KSCN 52.00 uL 0.5 M isn 38.00 ul H2O	5.00 uL 1 M Ni nitrate 5.00 uL 2 M KSCN 50.00 uL 0.5 M isn 40.00 ul H2O	5.00 uL 1 M Ni nitrate 5.00 uL 2 M KSCN 48.00 uL 0.5 M isn 42.00 ul H2O	5.00 uL 1 M Ni nitrate 5.00 uL 2 M KSCN 46.00 uL 0.5 M isn 44.00 ul H2O	5.00 uL 1 M Ni nitrate 5.00 uL 2 M KSCN 44.00 uL 0.5 M isn 46.00 ul H2O	5.00 uL 1 M Ni nitrate 5.00 uL 2 M KSCN 42.00 uL 0.5 M isn 48.00 ul H2O	5.00 uL 1 M Ni nitrate 5.00 uL 2 M KSCN 40.00 uL 0.5 M isn 50.00 ul H2O
C	5.00 uL 1 M Ni nitrate 5.00 uL 2 M KSCN 38.00 uL 0.5 M isn 52.00 ul H2O	5.00 uL 1 M Ni nitrate 5.00 uL 2 M KSCN 36.00 uL 0.5 M isn 54.00 ul H2O	5.00 uL 1 M Ni nitrate 5.00 uL 2 M KSCN 34.00 uL 0.5 M isn 56.00 ul H2O	5.00 uL 1 M Ni nitrate 5.00 uL 2 M KSCN 32.00 uL 0.5 M isn 58.00 ul H2O	5.00 uL 1 M Ni nitrate 5.00 uL 2 M KSCN 30.00 uL 0.5 M isn 60.00 ul H2O	5.00 uL 1 M Ni nitrate 5.00 uL 2 M KSCN 28.00 uL 0.5 M isn 62.00 ul H2O	5.00 uL 1 M Ni nitrate 5.00 uL 2 M KSCN 26.00 uL 0.5 M isn 64.00 ul H2O	5.00 uL 1 M Ni nitrate 5.00 uL 2 M KSCN 24.00 uL 0.5 M isn 66.00 ul H2O
D	5.00 uL 1 M Ni nitrate 5.00 uL 2 M KSCN 22.00 uL 0.5 M isn 68.00 ul H2O	5.00 uL 1 M Ni nitrate 5.00 uL 2 M KSCN 20.00 uL 0.5 M isn 70.00 ul H2O	5.00 uL 1 M Ni nitrate 5.00 uL 2 M KSCN 18.00 uL 0.5 M isn 72.00 ul H2O	5.00 uL 1 M Ni nitrate 5.00 uL 2 M KSCN 16.00 uL 0.5 M isn 74.00 ul H2O	5.00 uL 1 M Ni nitrate 5.00 uL 2 M KSCN 14.00 uL 0.5 M isn 76.00 ul H2O	5.00 uL 1 M Ni nitrate 5.00 uL 2 M KSCN 12.00 uL 0.5 M isn 78.00 ul H2O	5.00 uL 1 M Ni nitrate 5.00 uL 2 M KSCN 10.00 uL 0.5 M isn 80.00 ul H2O	5.00 uL 1 M Ni nitrate 5.00 uL 2 M KSCN 8.00 uL 0.5 M isn 82.00 ul H2O

Table S1.2. Final concentrations for crystallization screening.

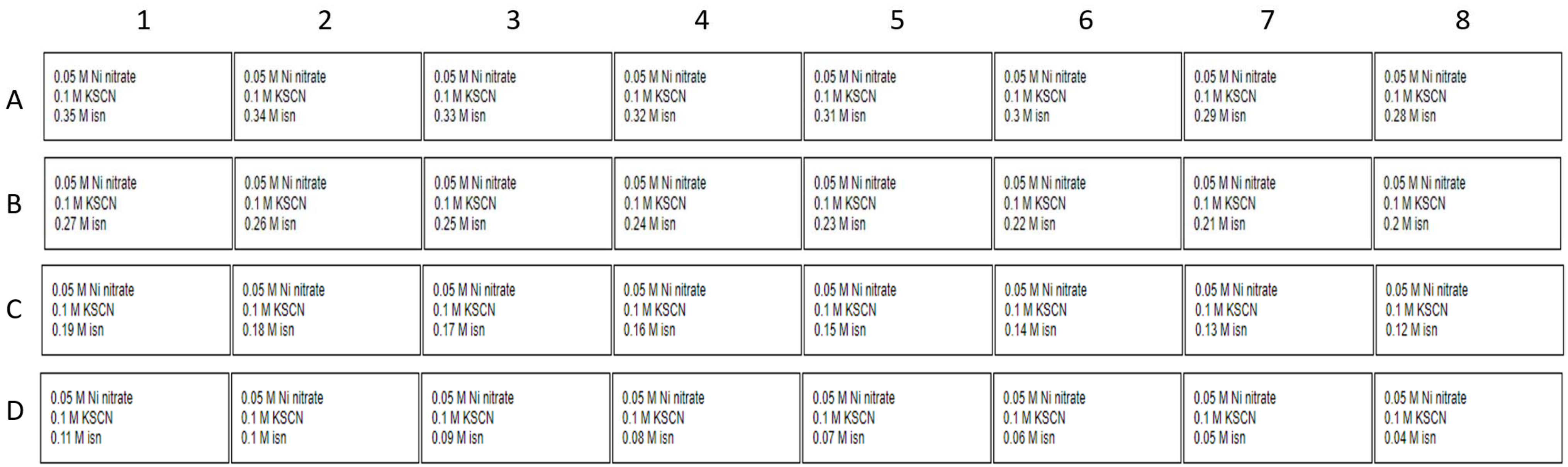

	1	2	3	4	5	6	7	8
A	0.05 M Ni nitrate 0.1 M KSCN 0.35 M isn	0.05 M Ni nitrate 0.1 M KSCN 0.34 M isn	0.05 M Ni nitrate 0.1 M KSCN 0.33 M isn	0.05 M Ni nitrate 0.1 M KSCN 0.32 M isn	0.05 M Ni nitrate 0.1 M KSCN 0.31 M isn	0.05 M Ni nitrate 0.1 M KSCN 0.3 M isn	0.05 M Ni nitrate 0.1 M KSCN 0.29 M isn	0.05 M Ni nitrate 0.1 M KSCN 0.28 M isn
B	0.05 M Ni nitrate 0.1 M KSCN 0.27 M isn	0.05 M Ni nitrate 0.1 M KSCN 0.26 M isn	0.05 M Ni nitrate 0.1 M KSCN 0.25 M isn	0.05 M Ni nitrate 0.1 M KSCN 0.24 M isn	0.05 M Ni nitrate 0.1 M KSCN 0.23 M isn	0.05 M Ni nitrate 0.1 M KSCN 0.22 M isn	0.05 M Ni nitrate 0.1 M KSCN 0.21 M isn	0.05 M Ni nitrate 0.1 M KSCN 0.2 M isn
C	0.05 M Ni nitrate 0.1 M KSCN 0.19 M isn	0.05 M Ni nitrate 0.1 M KSCN 0.18 M isn	0.05 M Ni nitrate 0.1 M KSCN 0.17 M isn	0.05 M Ni nitrate 0.1 M KSCN 0.16 M isn	0.05 M Ni nitrate 0.1 M KSCN 0.15 M isn	0.05 M Ni nitrate 0.1 M KSCN 0.14 M isn	0.05 M Ni nitrate 0.1 M KSCN 0.13 M isn	0.05 M Ni nitrate 0.1 M KSCN 0.12 M isn
D	0.05 M Ni nitrate 0.1 M KSCN 0.11 M isn	0.05 M Ni nitrate 0.1 M KSCN 0.1 M isn	0.05 M Ni nitrate 0.1 M KSCN 0.09 M isn	0.05 M Ni nitrate 0.1 M KSCN 0.08 M isn	0.05 M Ni nitrate 0.1 M KSCN 0.07 M isn	0.05 M Ni nitrate 0.1 M KSCN 0.06 M isn	0.05 M Ni nitrate 0.1 M KSCN 0.05 M isn	0.05 M Ni nitrate 0.1 M KSCN 0.04 M isn

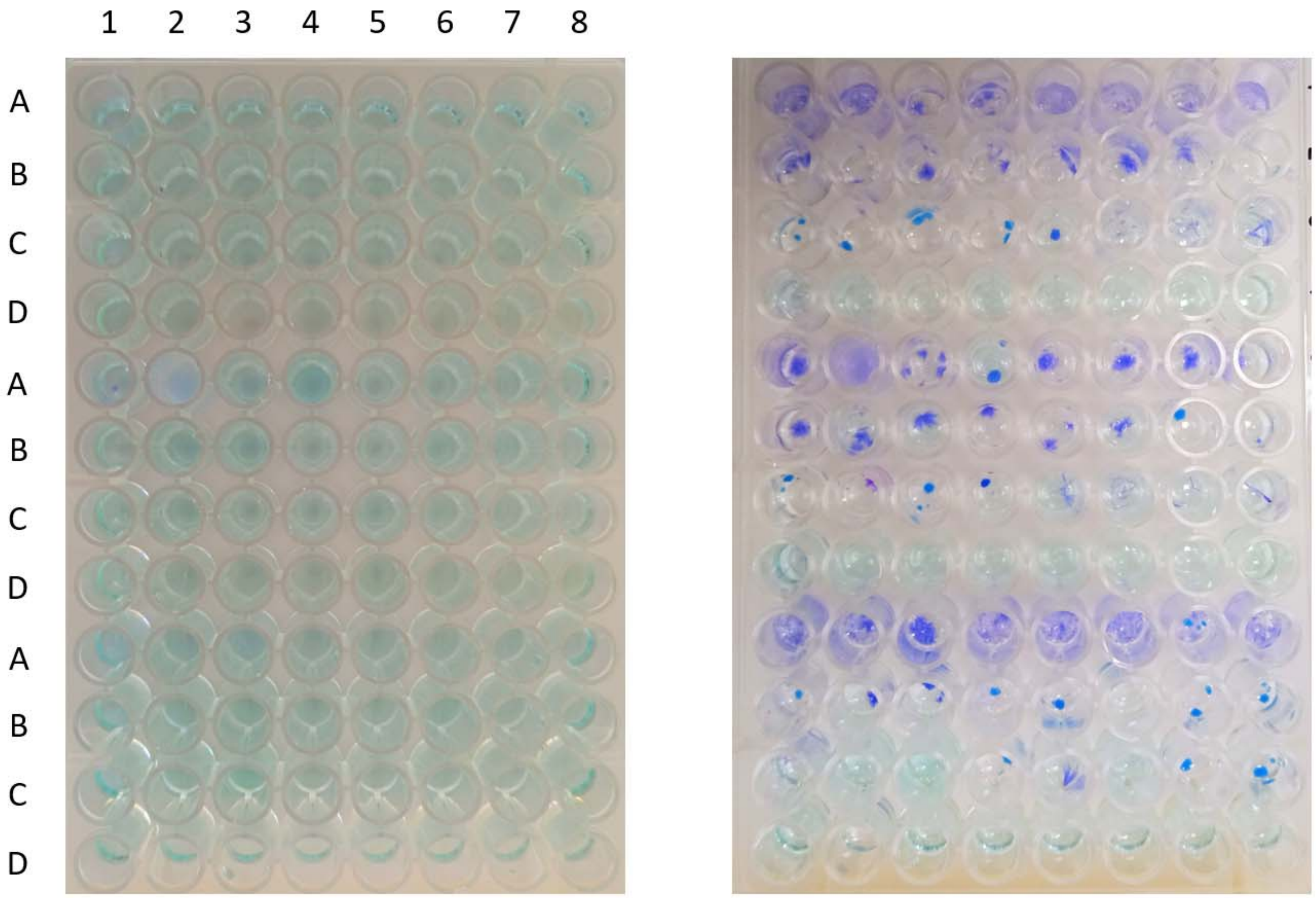

a

b

Figure S1.1. a) Crystallization plate after mixing the reactants; b) 14 days later.

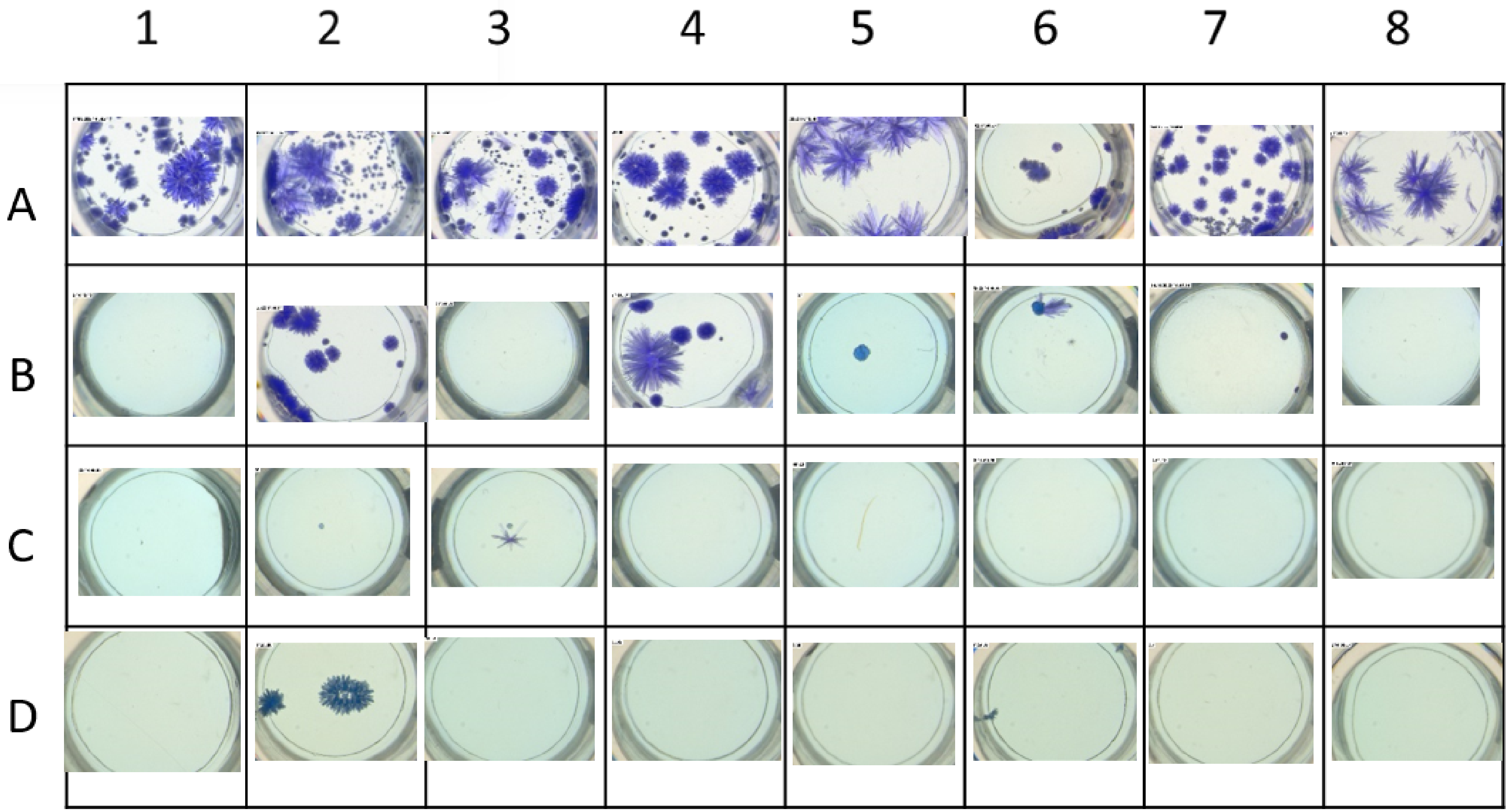

Figure S1.2. One set of crystallization conditions in a crystallization plate 1 day after mixing the reactants.

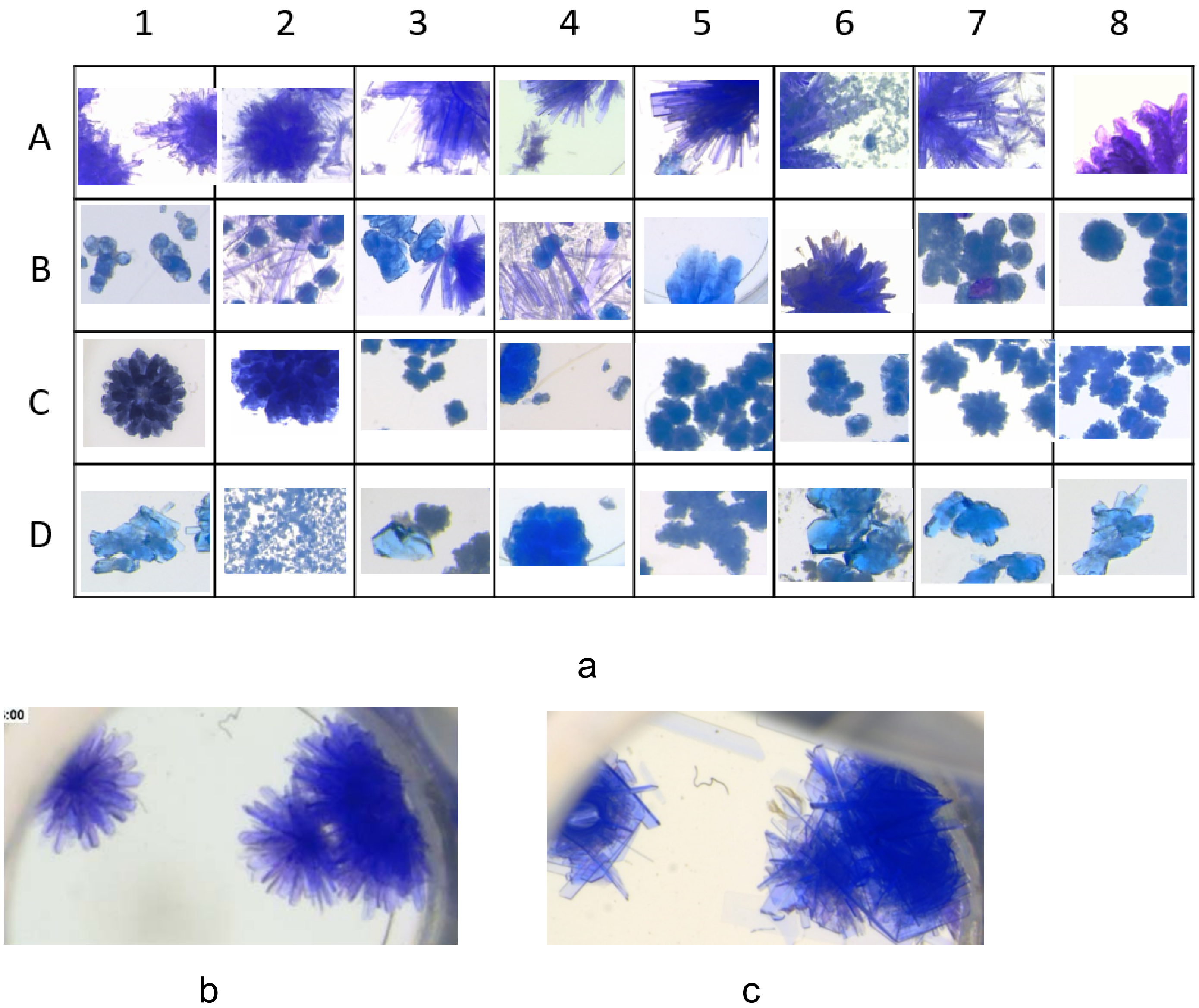

Figure S1.3. a) One set of crystallization conditions in a crystallization plate 1 month after mixing the reactants; b) **3a** in condition B5 in one crystallization plate; c) **4** in the same reservoir after partial dissolving and transformation.

Table S2. Crystal data and details of the structure determination for $[Ni(NCS)_2(isn)_2(H_2O)_2]\cdot 2H_2O$ (**1**), $[Ni(NCS)_2(isn)_2(H_2O)_2]$ (**2**), $[Ni(isn)_3(NCS)_2(H_2O)]\cdot 2.5H_2O$ (**3**), $[Ni(NCS)_2(isn)_3(H_2O)]\cdot 3[Ni(NCS)_2(isn)_4]\cdot 9H_2O$ (**4**), $[Ni(NCS)_2(isn)_4]\cdot 3H_2O$ (**5**) and $[Ni(NCS)_2(isn)_4]\cdot 2(isn)$ (**6**).

	$[Ni(NCS)_2(isn)_2(H_2O)_2]\cdot 2H_2O$ 1	**$[Ni(NCS)_2(isn)_2(H_2O)_2]$ 2**	**$[Ni(NCS)_2(isn)_3(H_2O)]\cdot 2.5H_2O$ 3**	**$[Ni(NCS)_2(isn)_3(H_2O)]\cdot 3[Ni(NCS)_2(isn)_4]\cdot 9H_2O$ 4**	**$[Ni(NCS)_2(isn)_4]\cdot 3H_2O$ 5**	**$[Ni(NCS)_2(isn)_4]\cdot 2(isn)$ 6**
Crystal data						
Chemical formula	**$C_{14}H_{20}$ $N_6NiO_6S_2$**	**$C_{14}H_{16}N_6NiO_4S_2$**	**$C_{20}H_{25}N_8NiO_{6.5}S_2$**	**$C_{98}H_{110}N_{38}Ni_4O_{25}S_8$**	**$C_{26}H_{30}N_{10}NiO_7S_2$**	**$C_{38}H_{36}N_{14}NiO_6S_2$**
Formula weight M_r	491.19	455.16	604.31	2711.55	717.43	907.64
Crystal system. space group	Monoclinic. $P2_1/c$	Monoclinic. $P2_1/c$	Monoclinic. $C2/c$	Triclinic. $P\bar{1}$	Orthorhombic. *Pbcn*	Triclinic. $P\bar{1}$
Crystal size (mm)	0.06 × 0.25 × 0.44	0.04 × 0.05 × 0.12	0.06 × 0.15 × 0.21	0.11 × 0.07 × 0.04	0.09 × 0.25 × 0.28	0.08 × 0.09 × 0.21
Crystal habit. colour	Plate. blue	Prism. cyan	Prism. light blue	Plate. blue	Prism. purple	Rod-like prismatic, violet
Temperature (K) and ambient_environment for data collection	296	170	170	170	170	170
a; b; c (Å)	11.3044(7); 7.5445(4); 14.5600(8)	10.4266(1); 13.2360(1); 7.1637(1)	19.2685(7); 13.0098(5); 20.5857(7)	15.5300(2); 18.8935(1); 22.3982(2)	18.2189(2); 20.4103(2); 8.4405(1)	9.13447(14); 13.5769(2); 20.2632(3)
α; β; γ (°)	90; 123.000(5); 90	90; 104.165(1); 90	90; 96.725(3); 90	83.188(1); 71.670(1); 86.988(1)	90; 90; 90	70.5876(14); 82.6375(13); 71.1381(14)
V (Å^3)	1041.43(12)	958.58(2)	5124.9(3)	6193.69(11)	3138.63(6)	2242.25(6)
Z	2	2	8	2	4	2
D_{calc} (Mg m^{-3})	1.566	1.577	1.566	1.454	1.518	1.344
μ (mm^{-1})	1.18	3.80	3.10	2.64	2.67	2.00
F(000)	508	468	2504	2808	1488	940
Data collection						
Diffractometer	Oxford Diffraction Xcalibur difractometer with Sapphire3 detector	XtaLAB Synergy. Dualflex. HyPix diffractometer	XtaLAB Synergy. Dualflex. HyPix diffractometer	XtaLAB Synergy. Dualflex. HyPix diffractometer	XtaLAB Synergy. Dualflex. HyPix diffractometer	XtaLAB Synergy. Dualflex. HyPix diffractometer
Radiation type	Mo *Kα*. λ=0.71073 Å	Cu *Kα*. λ=1.5418 Å	Cu *Kα*. λ=1.5418 Å	Cu *Kα*. λ=1.5418 Å	Cu *Kα*. λ=1.5418 Å	Cu *Kα*. λ=1.5418 Å
Absorption correction	multi-scan- *CrysAlis RED*. Oxford Diffraction Ltd.. Version 1.171.31.5 (release 28-08-2006 CrysAlis171 .NET) (compiled Aug 28 2006.13:05:05) Empirical absorption correction using spherical harmonics. implemented in SCALE3 ABSPACK scaling algorithm.	multi-scan - *CrysAlis PRO* 1.171.41.92a (Rigaku Oxford Diffraction. 2020) Empirical absorption correction using spherical harmonics. implemented in SCALE3 ABSPACK scaling algorithm.	multi-scan - *CrysAlis PRO* 1.171.41.92a (Rigaku Oxford Diffraction. 2020) Empirical absorption correction using spherical harmonics. implemented in SCALE3 ABSPACK scaling algorithm.	multi-scan - *CrysAlis PRO* 1.171.41.92a (Rigaku Oxford Diffraction. 2020) Empirical absorption correction using spherical harmonics. implemented in SCALE3 ABSPACK scaling algorithm.	multi-scan - *CrysAlis PRO* 1.171.41.92a (Rigaku Oxford Diffraction. 2020) Empirical absorption correction using spherical harmonics. implemented in SCALE3 ABSPACK scaling algorithm.	multi-scan - *CrysAlis PRO* 1.171.41.92a (Rigaku Oxford Diffraction. 2020) Empirical absorption correction using spherical harmonics. implemented in SCALE3 ABSPACK scaling algorithm.
T_{min}; T_{max} for absorption correction	0.734; 0.933	0.457; 1.000	0.754; 1.000	0.497; 1.000	0.735; 1.000	0.821; 1.000
R_{int}	0.021	0.038	0.047	0.061	0.043	0.038
(sin $\theta/\lambda)_{max}$ (Å^{-1})	0.703	0.633	0.602	0.626	0.635	0.634
θ_{min}–θ_{max} (°) (No. of reflections used to measure unit cell) Temperature (K)	3.7–36.5 (11347) 296	3.3–77.3 (9419) 170	4.3–79.6 (12170) 170	3.0–77.3 (61185) 170	3.3–77.2 (18948) 170	3.6–77.3 (23831) 174
θ range for data collection (°)	3.9−30.0	4.4−77.4	4.1−68.2	3.0−75.0	3.3−78.0	4.6−78.0
h.k.l range	−15:15. −10:10. −20:20	−12:13. −16:16. −8:9	−23:23. −15:15. −19:24	−19:19. −23:21. −28:28	−22:23. −25:25. −10:8	−10:11. −15:17. −25:25
Scan type	ω	ω	ω	ω	ω	ω
No. measured. independent and observed. $I \geq 2\sigma(I)$reflections	22838. 3027. 2434	11848. 2007. 1950	16963. 4636. 4127	94929. 25160. 22708	29980. 3319. 3147	37940. 9376. 8436

Refinemant on F^2						
No. of refined parameters	158	131	371	1558	224	551
No. of restraints	none	4	10	8	6	none
H-atom treatment	[!] H-atom parameters constrained	[!!] H-atom parameters constrained	[!!] H-atom parameters constrained	[!!] H-atom parameters constrained	[!!] H-atom parameters constrained	[!!!] H-atom parameters constrained
R [all data]; R^a [$I \geq 2\sigma(I)$]	0.039; 0.029	0.027; 0.027	0.060; 0.056	0.079; 0.069	0.031; 0.030	0.037; 0.034
wR [all data]; $wR^{b,c}$ [$I \geq 2\sigma(I)$]	0.080; 0.073	0.073; 0.073	0.172; 0.168	0.172; 0.170	0.080; 0.079	0.090; 0.088
Weighting parameters [c] g_1; g_2	0.0389; 0.3275	0.0432; 0.3753	0.1135; 11.7373	0.0242; 30.5226	0.044; 1.2669	0.0418; 0.6851
Goodness of fit on F^2, S^d	1.05	1.071	1.04	1.11	1.05	1.06
Max.; min. electron density, $\Delta\rho_{max}$; $\Delta\rho_{min}$ (eÅ^{-3})	0.59; − 0.54	0.41; − 0.30	1.43; − 0.76	1.26; − 0.65	0.32; − 0.48	0.29; − 0.33
Extinction coefficient, x^e	0.0042(11)	0.0041(4)	none	0.000115(16)	none	0.00033(9)

*Multi-scan *CrysAlis RED*. Oxford Diffraction Ltd.. Version 1.171.32.4 (release 27-04-2006 CrysAlis171 .NET) (compiled Apr 27 2007.17:53:11) Empirical absorption correction using spherical harmonics. implemented in SCALE3 ABSPACK scaling algorithm.

[!] A riding model with $U_{iso}(H) = 1.2U_{eq}(C)$ and with C—H = 0.95 Å for aromatic H atoms. The water and amide H atoms were refined freely with isotropic factor U_{iso}.

[!!] A riding model with $U_{iso}(H) = 1.2U_{eq}$(C or N) and with C—H = 0.95 Å for aromatic and N—H = 0.88 Å for amide H atoms. The water H atoms were refined using DFIX distance restraints with O—H = 0.85 Å. H1—H2 = 1.37 Å and $U_{iso}(H) = 1.5U_{eq}(O)$.

[!!!] A riding model with $U_{iso}(H) = 1.2U_{eq}$(C or N) and with C—H = 0.95 Å for aromatic and N—H = 0.88 Å for amide H atoms.

[a] $R = \Sigma[\,|\,|F_o| - |F_c|\,|\,]/\Sigma|F_o|$; [b] $wR = \{\Sigma[w(F_o^2 - F_c^2)^2]/\Sigma[w(F_o^2)^2]\}^{½}$; [c] $w = 1/[\sigma^2(F_o^2) + (g_1P)^2 + g_2P]$ where $P = (F_o^2 + 2F_c^2)/3$; [d] $S = \{\Sigma[w(F_o^2 - F_c^2)^2]/(N_{obs} - N_{param})\}^{½}$; [e] $F_c^* = kF_c[1 + 0.001xF_c^2\lambda^3/\sin(2\theta)]^{-¼}$ where k is the overall scale fact

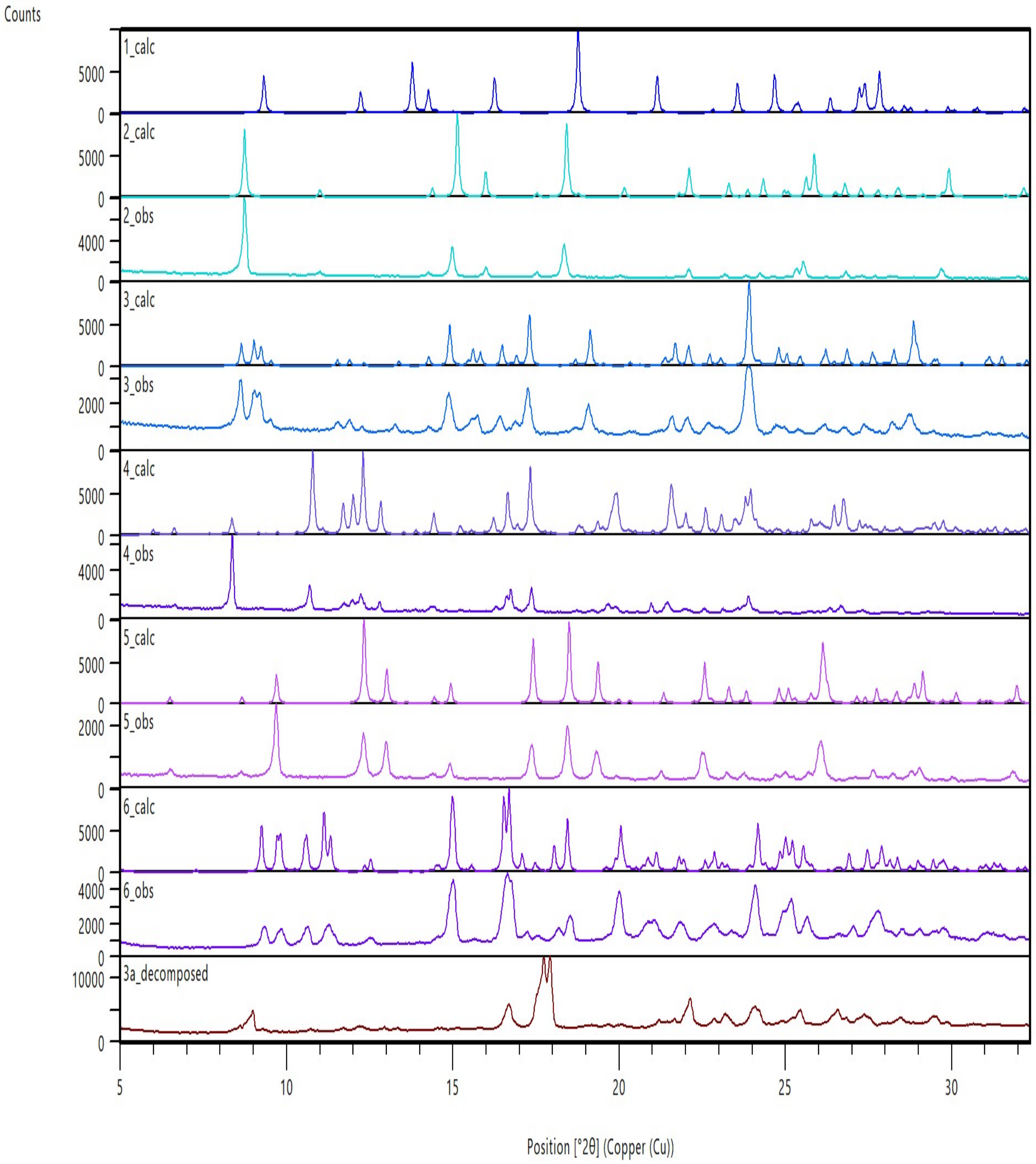

Figure S2. Calculated powder diffraction pattern of **1**, and calculated and observed patterns for **2**–**6**.

Table S3. The dihedral angles between pyridine ring and amide group (°) in complexes **1**–**6**.

	py plane	**am plane**	**angle (°)**
1	N11C12-C16	C14C17O11N12	23.140(5)
2	N11C12-C16	C14C17O11N12	18.11(3)
3	N11C12-C16	C14C17O11N12	3.6(4)
	N21C22-C26	C24C27O21N22	24.9(4)
	N31C32-C36	C34C37O31N32	23.7(3)
4	N11C12-C16	C14C17O11N12	6.1(3)
	N21C22-C26	C24C27O21N22	28.8(2)
	N31C32-C36	C34C37O31N32	6.7(3)
	N41C42-C46	C44C47O41N42	19.3 (2)
	N51C52-C56	C54C57O51N52	26.9(2)
	N61C62-C66	C64C67O61N62	6.0(3)
	N71C72-C76	C74C77O71N72	23.0(3)
	N81C82-C86	C84C87O81N82	20.6(2)
	N91C92-C96	C94C97O91N92	12.8(2)
	N101C102-C106	C104C107O101N102	2.6(3)
	N111C112-C116	C114C117O111N112	34.1(2)
	N121C122-C126	C124C127O121N122	11.9(2)
	N131C132-C136	C134C137O131N132	19.0(3)
	N141C142-C146	C144C147O141N142	23.2(3)
	N151C152-C156	C154C157O151N152	13.7(2)
5	N11C12-C16	C14C17O11N12	39.96(6)
	N21C22-C26	C24C27O21N22	43.40(6)
6	N11C12-C16	C14C17O11N12	3.0(1)
	N21C22-C26	C24C27O21N22	2.1(1)
	N31C32-C36	C34C37O31N32	4.0(1)
	N41C42-C46	C44C47O41N42	7.96(9)
	N51C52-C56	C54C57O51N52	35.49(6)
	N61C62-C66	C64C67O61N62	28.84(7)

Table S4. Selected bond distances (Å) and angles (°) in and between thiocyanate ligand including Ni–N–C angles of the complexes **1**–**6**.

	1	**2**	**3**	**4**				**5**	**6**
S–C	1.6326 (17)	1.6427 (14)	1.638(3); 1.633(3)	1.630 (5); 1.633 (5) ; 1.631 (10)	1.634 (4); 1.632 (4)	1.648 (4); 1.632 (5)	1.642 (4); 1.643 (5)	1.6408(14)	1.6355(14); 1.6363(15)
C–N	1.153(2)	1.1578 (18)	1.161(4); 1.161(4)	1.161 (6); 1.209 (7); 1.187 (13)	1.156 (6); 1.162 (5)	1.158 (5); 1.168 (6)	1.148 (5); 1.155 (5)	1.1599(18)	1.1620(19); 1.1597(19)
S–C–N	178.74(19)	178.31 (13)	177.4(3); 179.4(3)	177.8 (4); 178.7 (5); 155 (2)	179.2 (4); 178.9 (4)	178.9 (4); 177.2 (4)	177.3 (4); 179.3 (4)	178.81 (12)	178.56(13); 178.95(14)
Ni–N–C	164.93 (16)	169.88 (11)	161.6 (3); 169.2(2)	158.2 (4); 145.8 (4); 145 (1)	166.2 (3); 151.2 (3)	154.4 (3); 148.7 (4)	150.2 (3); 162.4 (3)	178.40(10)	155.80(11); 166.61 (12)

Table S5. The bond distances (Å) and angles (°) in the carboxamide group of the complexes **1**–**6**.

		1	**2**	**3**	**5**	**6**
coordinated	C = O	1.228(2)	1.2357 (17)	1.223(4); 1.246(4); 1.227(4)	1.2355(17); 1.2281(17)	1.2326(17); 1.2340(18); 1.2308(19); 1.2300(18)
	C – N	1.321(3)	1.3250 (17)	1.335(4); 1.319(4); 1.330(4)	1.3302(18); 1.3334(17)	1.3289(19); 1.3271(19); 1.324(2); 1.3351(19)
	O – C – N	122.0(2)	122.57 (12)	121.9(3); 122.6(3); 122.9(3)	123.07(12); 123.93(12)	121.88(13); 122.88(14); 122.98(14); 122.41(13)
uncoordinated	C = O	-	-	-	-	1.2501(17); 1.232(2)
	C – N	-	-	-	-	1.3173(19); 1.329(2)
	O – C – N	-	-	-	-	123.52(13); 123.19(14)
		4				
coordinated	C = O	1.235(6); 1.236(5); 1.236(6); 1.231(5); 1.239(5); 1.235(6); 1.223(5); 1.233(5); 1.238(5); 1.235(5); 1.245(6); 1.244(5); 1.224(5); 1.234(5); 1.232(5)				
	C – N	1.321(7); 1.327(5); 1.322(6); 1.321(5); 1.329(6); 1.320(6); 1.353(6); 1.328(6); 1.331(5); 1.321(6); 1.328(6); 1.315(5); 1.331(6); 1.330(6); 1.325(5)				
	O – C – N	122.5(5); 122.6(4); 121.5(4); 123.1(4); 122.8(4); 123.7(4); 122.2(4); 122.6(4); 122.5(4); 122.1(4); 122.8(4); 122.0(4); 122.7(4); 123.1(4); 122.7(4)				

Discussion S1. Additional analysis of the molecular structures 1–6.

$[Ni(NCS)_2(isn)_2(H_2O)_2]\cdot 2H_2O$ (1)

The amide –C(=O11)N12H_2 group plane is out of the pyridine ring plane and they mutually close the dihedral angle of 23.140(5)° (Table S3). The NCS^- groups show almost linearity having N1—C1—S1 angle of 178.74(19)° (Table S4). The bond distances (Å) and angles (°) in the carboxamide group are shown in Table S5. The relatively large U_{eq} of 0.0951(9) $Å^2$ for weakly bound uncoordinated water oxygen O2 indicate a disorder in that part of structure.

$[Ni(isn)_2(NCS)_2(H_2O)_2]$ (2)

The molecular structure of **2** is similar to that of **1**, which is the hydrate form, with only somewhat different geometrical parameters (Table 1 and Tables S3-S5). A slightly distorted octahedral coordination geometry around Ni(II) are constituted by two symmetry equivalent pyridine ring nitrogen N11 atoms of coordinated isonicotinamide ligands, two nitrogen N1 atoms of anionic thiocyanate ligands and two oxygen O1 atoms of water molecules. In the anhydrous structure of **2**, the dihedral angle between the pyridine ring and the amide group is 18.11(3)° which is slightly smaller than 23.140(5)° in **1** (Table S3).

$[Ni(NCS)_2(isn)_3(H_2O)]\cdot 2.5H_2O$ (3)

The $NiN_5(OH_2)$ octahedral coordination of metal centre is formed by three pyridine ring nitrogen N11, N21, N31 atoms from three isonicotinamide ligands, two thiocyanate nitrogen N1 and N2 atoms at slightly shorter distances from two equatorially *trans* N-bonded thiocyanate ligands and one water molecule oxygen O1 (Table 1). The bond angles around the central metal ion deviate slightly from the ideal octahedral molecular geometry [*cis*-angles: 85.96(9)–94.17(11)° and *trans*-angles: 174.44(10)–178.11(9)°]. The bond distances in the almost perfect $NiN_5(OH_2)$ octahedra are expectedly slightly shorter than in its cobalt analogue.

Two amide groups –C(=O31)N32H_2 and –C(=O21)N22H_2 in two isonicotinamide ligands (Figure 4a) that are *cis*-positioned one to another, were rotated by 23.7(3)° and 24.9(4)° respectively, relative to the pyridine ring mean plane to which they are attached, compared to 3.7(4)° for the third amide –C(=O11)N12H_2 (Table S3). Both NCS-groups (Table S4) show almost linearity having N1–C1–S1 angle of 177.4(3)°, N2–C2–S2 angle of 179.4(3)° and typical bond distances (N1–C1 = 1.161(4); C1–S1 = 1.638(3); N2–C2 = 1.161(4) and C2–S2 = 1.633(3) Å). The bond distances (Å) and angles (°) in the carboxamide groups are given in Table S5.

$[Ni(NCS)_2(isn)_3(H_2O)]\cdot 3[Ni(NCS)_2(isn)_4]\cdot 9H_2O$ (4)

The Ni—N bond lengths to the thiocyanate anions are slightly shorter than those to the pyridine N atoms, which is in agreement with values for similar structures (Table 1). Average bond lengths vary in narrow ranges and are 2.098, 2.100, 2.107 and 2.105 Å for Ni1N_{2+3}O, Ni2N_{2+4}, Ni3N_{2+4} and Ni4N_{2+4} octahedra, respectively. The bond angles around the Ni(II) cations deviate somewhat from ideal values. They occur from 87.1(1) to 93.9(1)° and from 174.3(1) to 178.4(1)° for *cis* and *trans* angles, respectively, showing that the octahedra are slightly distorted. Isonicotinamide ligands act as monodentate ligands and are coordinating Ni(II) cations through nitrogen atoms of pyridine rings. For each isonicotinamide ligand, the amide group is rotated differently out of the pyridine ring plane, with dihedral angles ranging from 6.0(3) to 34.1(2)° (Table S3). Thiocyanate anions NCS^- act as terminal ligands and are coordinating Ni(II) cations also through the nitrogen atom. One of eight NCS^- groups in the asymmetric unit exhibited positional disorder. Atoms C2 and S2 were disordered over two positions (N2C2aS2a and N2C2bS2b) with the major component contributing 82.0(4)%. The connections between Ni atoms and NCS^- groups are slightly bent with Ni—N—C angles ranging from 145(1) to 166.2(3)° (Table S4). The NCS^- groups show almost linearity with N—C—S angles varying from 177.3(4) to 179.3(4)° (Table S4).

$[Ni(NCS)_2(isn)_4]\cdot 3H_2O$ (5)

The central metal ion Ni(II) and its attached ligands form slightly distorted octahedron. The individual bond lengths Ni—N are in the narrow range from 2.0554(11) to 2.1238(10) Å. while N—Ni—N angles occur from 89.08(6) to 91.79(6)° and from 178.43(4) to 179.78(6)° for *cis* and *trans* angles, respectively.

[Ni(NCS)$_2$(isn)$_4$]·2(isn) (6)

The central metal ions Ni(II) are coordinated by six N atoms, four from isonicotinamide ligands in equatorial, and 2 from terminal bonded thiocyanate anions in axial positions (Figure 8a). Bond lengths [Ni—N range: 2.0517(12)–2.1305(11) Å] and angles [N—Ni—N range: 88.29(4)–91.38(5)° for *cis* and 178.39(5)–178.93(5)° for *trans* angles] illustrate a low octahedral distortion of NiN$_6$ octahedra (Table 1 and Tables S3-S5).

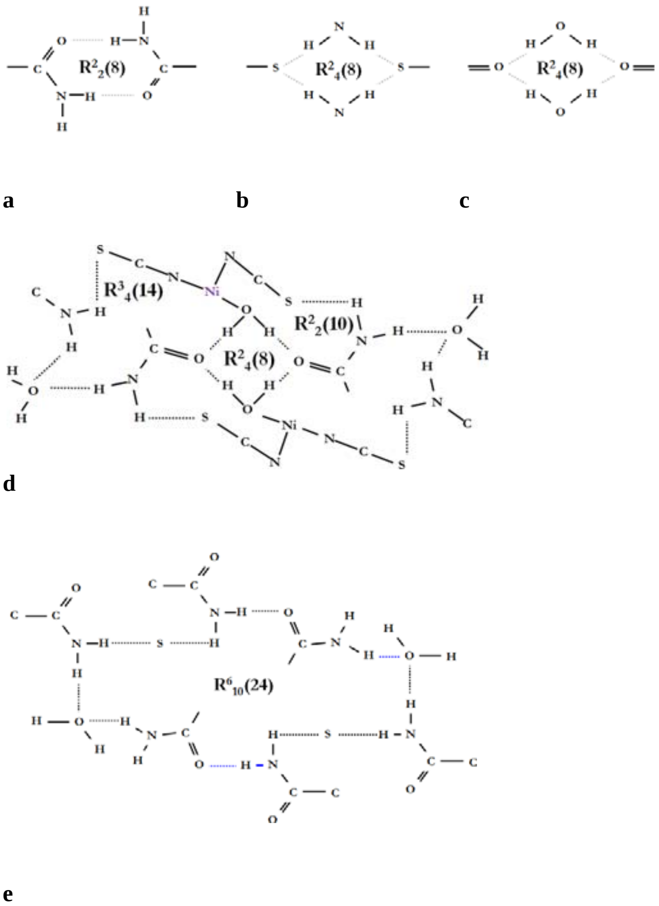

Scheme S1. Typical head-to-head amide-amide hydrogen bond $R^2_2(8)$ dimer in **3** (a). The $R^2_4(8)$ tetramer formed between the nitrogen atoms of the amide groups and the terminal thiocyanate sulphur atoms (b). The analogous $R^2_4(8)$ tetramer comprising the oxygen atoms of the amide groups instead of terminal thiocyanate and the coordinated water molecules found in complex **3** (c). Five fused rings of hydrogen bonding: $R^2_4(8)$ tetramer, two $R^3_4(14)$ tetramers and $R^2_2(10)$ dimers (d) and centrosymmetrical ring denoted by graph-set descriptor $R^6_{10}(24)$ (e) found in complex **3**.

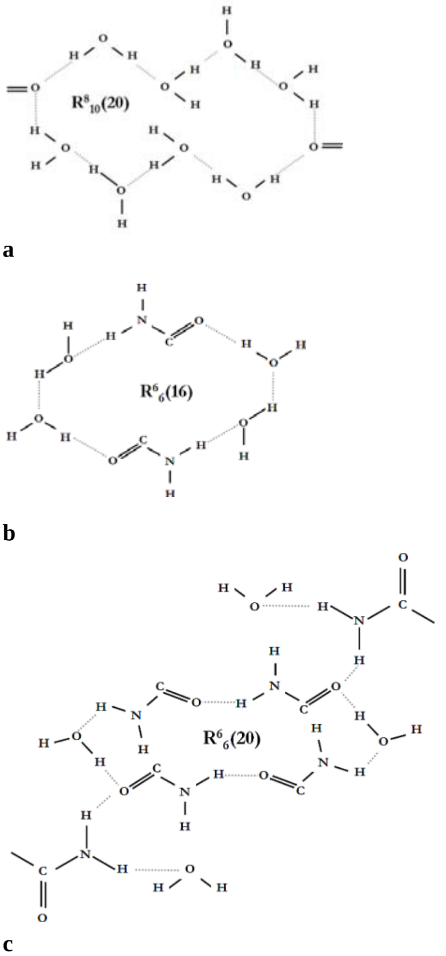

Scheme S2. The $R^8_{10}(20)$ decamer in **4** formed in the slab I between the two amide oxygen O atoms acting as double acceptor and eight water molecules (H_2O1-H_2O4 with their symmetry equivalents) acting as donor and acceptor around the inversion centre at 0.5 0 0 (a). The $R^6_6(16)$ hexamer formed in the slab I between the two amide groups and four water molecules (H_2O5 and H_2O6 with their symmetry equivalents) around the inversion centre at 0 0 0 (b). The $R^6_6(20)$ hexamer formed in the slab I between the four amide groups and two water molecules (H_2O6 with its symmetry equivalent) around the inversion centers at 0 0 0. A water molecule H_2O7 is attached to the hexameric ring *via* the fifth amide group (c).

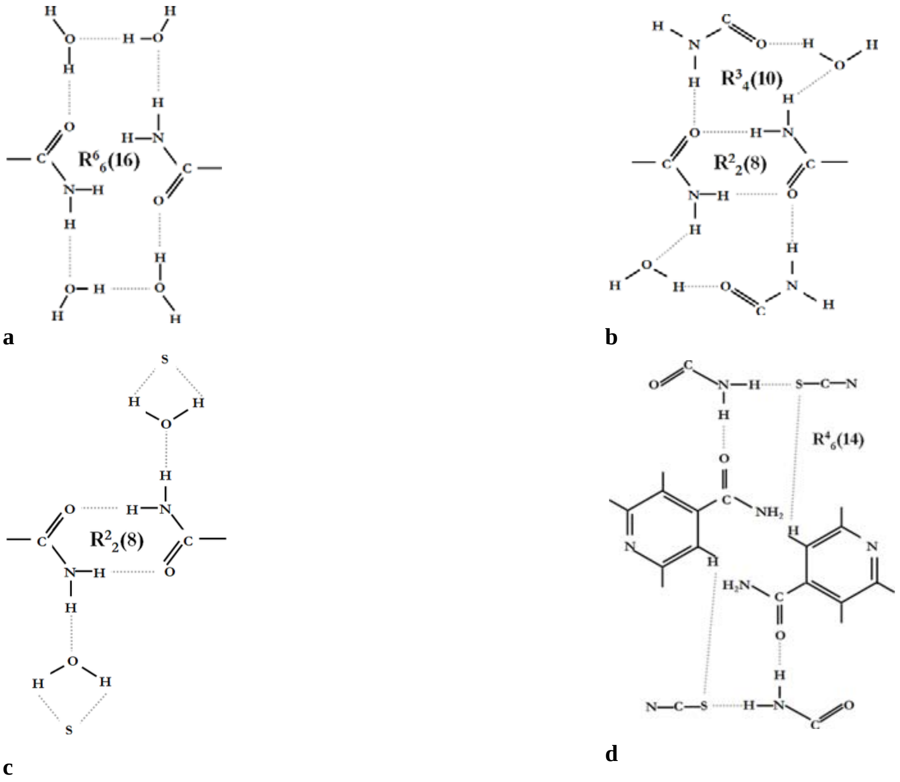

Scheme S3. The R$^6_6$(16) hexameric ring in **4** formed in the slab II between two amide groups and four water molecules (H_2O8 and H_2O9 with their symmetry equivalents) around the inversion centre at 0 0.5 0.5 (a). In the same slab II a typical head-to-head amide-amide hydrogen bond R$^2_2$(8) dimer in combination with two R$^3_4$(10) tetramers are found around the inversion centre at 0.5 0.5 0.5 (b). Again, the typical head-to-head amide-amide hydrogen bond R$^2_2$(8) dimer situated around the inversion centre at 0.5 0 0.5 was also found. The water molecules H_2O10 from slab II are further involved in weak intermolecular N—H···O and O—H···S hydrogen-bonding interactions (c). The R$^4_6$(14) ring formed by carboxamide groups —C(=O)NH_2 and thiocyanato sulphur S atom by the interactions of N—H···O and N—H···S type. Additionally, the thiocyanato sulphur S atom acts as a hydrogen bond acceptor for a weak hydrogen bonding interactions C—H···S type (d).

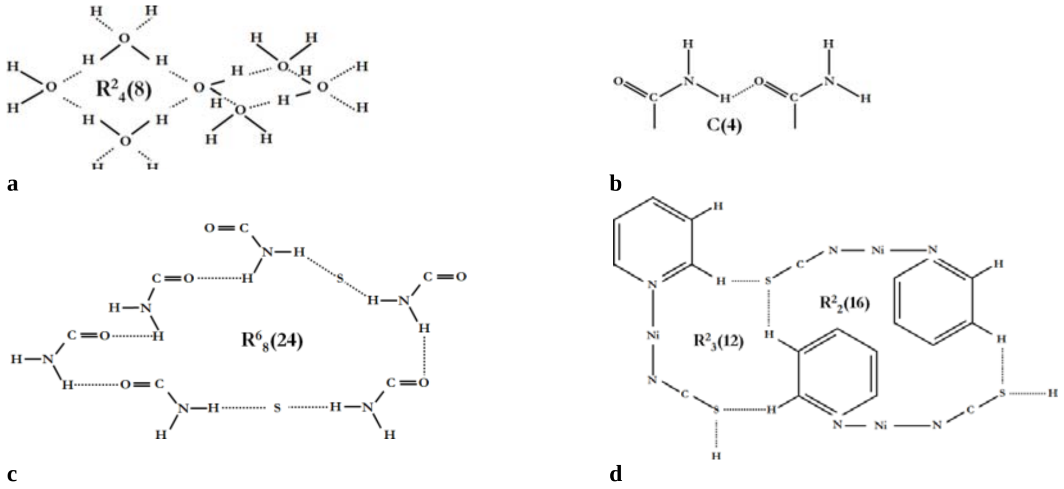

Scheme S4. The R$^2_4$(8) cyclic water tetramers linked in the zig-zag hydrogen bonded chain (a) and the carboxamide catemeric C(4) chains found in complex **5** (b). The R$^6_8$(24) ring formed by carboxamide groups —C(=O)NH$_2$ and thiocyanato sulphur S1 atom by the interactions of N—H···O and N—H···S type (c). Two fused rings of hydrogen bonding R$^2_3$(12) and R$^2_2$(16) where the thiocyanato sulphur S1 atom acts as a hydrogen bond acceptor for a weak hydrogen bonding interactions C—H···S type (*A*···*D* distances are 3.6430(13) Å).

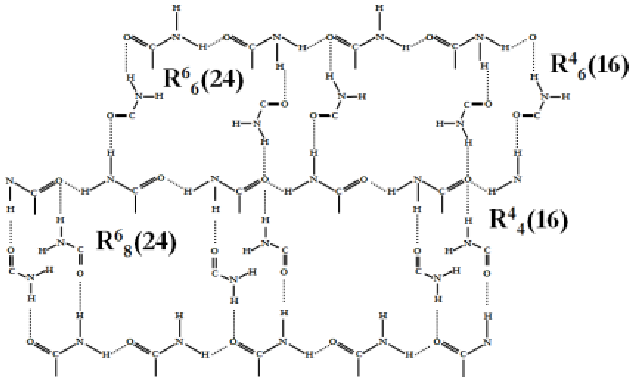

Scheme S5. A 2D corrugated sheet network in **6** as a combination of R$^4_4$(16), R$^4_6$(16), R$^6_6$(24) and R$^6_8$(24) graph-set motifs approximately along *c*-axis (*a*-axis is horizontal).

Discussion S2. Data collection and short crystal structure analysis for [Ni(NCS)$_2$(isn)$_4$]•1.25H$_2$O (7)

Data collection and short crystal structure analysis for [Ni(NCS)$_2$(isn)$_4$]·1.25H$_2$O (**7**). Blue crystals (Figure S6) crystallized in B2 conditions of the screening experiment. Single crystal X-ray diffraction revealed that **7,** $C_{26}H_{27}N_{10}NiO_{5.5}S_2$ crystallizes in the monoclinic non-centrosymmetric space group *Cc* [Flack x absolute structure parameter is –0.0078 (15)] with unit cell dimensions of a = 12.5286(3) Å, b = 31.4399(6) Å, c = 16.4687(3) Å and β = 110.301 (2)°, Z = 8, V = 6084.0(2). The crystal structure was solved and refined using F^2 values to R [$F^2 > 2\sigma(F^2)$] = 0.041, Rw = 0.101 for 8428 independent reflections (R_{int} = 0.048), and R = 0.044, Rw = 0.103 for all reflections, S = 1.04. PXRD was in agreement with the solved structure (Figure S7). The asymmetric unit consists of two discrete complex units [Ni(NCS)$_2$(isn)$_4$] and three co-crystallized water molecules (Figure S8). Both Ni(II) atoms are situated in general positions and are six-coordinated to two nitrogen atoms of *trans* positioned NCS$^-$ anions [Ni–N = 2.040(4)–2.067(4) Å] and four N atoms of the monodentate isonicotinamide ligands with bond distances Ni–N = 2.107(4)–2.174(4) Å, forming a slightly distorted octahedral geometry.

Co-crystallized water molecules are hydrogen bonded to the complex units in a three-dimensional hydrogen-bonding network formed by classical O—H···O as well as by N—H···O, C—H···O, O—H···N, O—H···S, N—H···N, N—H···S, C—H···N and C—H···S hydrogen bond interactions. The crystal packing is additionally consolidated and further stabilized by weak anion–π interactions indicated by the short distances between the centroids of the pyridine rings and O or S atoms of neighbouring molecules. The shortest π···O distance is 3.5621(1) Å and the range of the shortest π···S distances are from 3.3985(1) to 3.8454(1) Å. The centroid–centroid distances, which are equal or greater than 4.2204(1) Å, are probably too long for efficient π-stacking interactions.

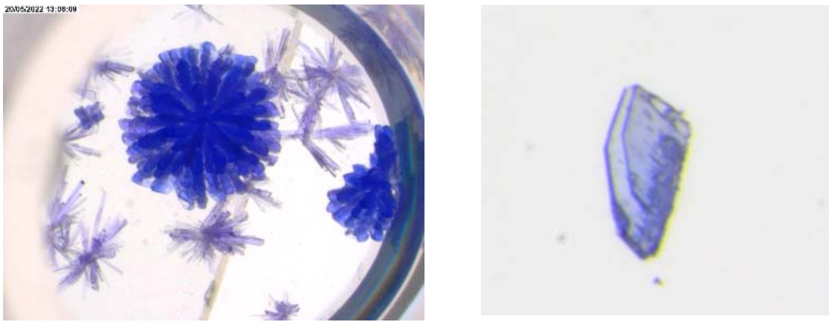

a b

Figure S3. a) Crystals of **7** (blue rosette) together with **6** in B2; b) two crystals of **7**.

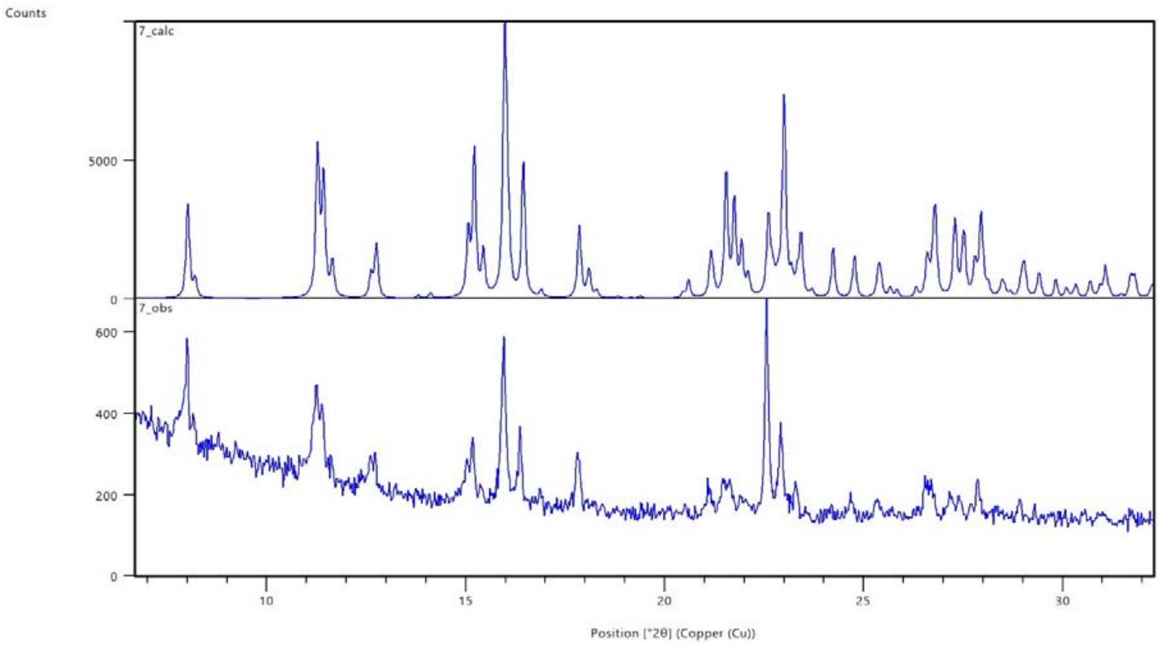

Figure S4. Powder diffraction patterns for **7**.

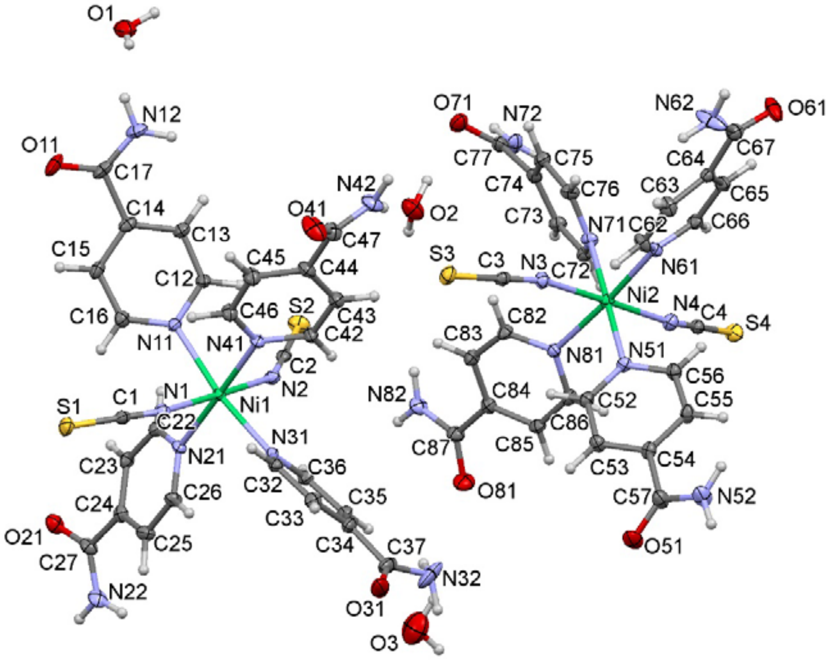

Figure S5. Molecular structure of $[Ni(NCS)_2(isn)_4]\cdot1.25H_2O$ (**7**) with the atom-numbering scheme.

Table S6. Thermogravimetric data of compounds **1**–**6**.

Compound	Water loss			Complex decomposition		
	θ / °C	$w_{\mathrm{theor}}(\mathrm{H_2O})$ / %	$w_{\mathrm{exp}}(\mathrm{H_2O})$ / %	θ / °C	$w_{\mathrm{theor}}(\mathrm{Ni})$ / %	$w_{\mathrm{exp}}(\mathrm{Ni})$ / %
1	67	14.67	14.31	200	11.95	/[a]
2	105	7.92	8.23	260	12.90	13.16
3	50	10.44	12.2	190	9.71	9.92
4[b]	42	6.64	4.12	170	8.66	10.7
5	45	7.53	6.91	172	8.18	8.54
6	/	0	0	160	6.47	6.67

[a] sample did not decompose completely; [b] sample partially decomposed before measurement

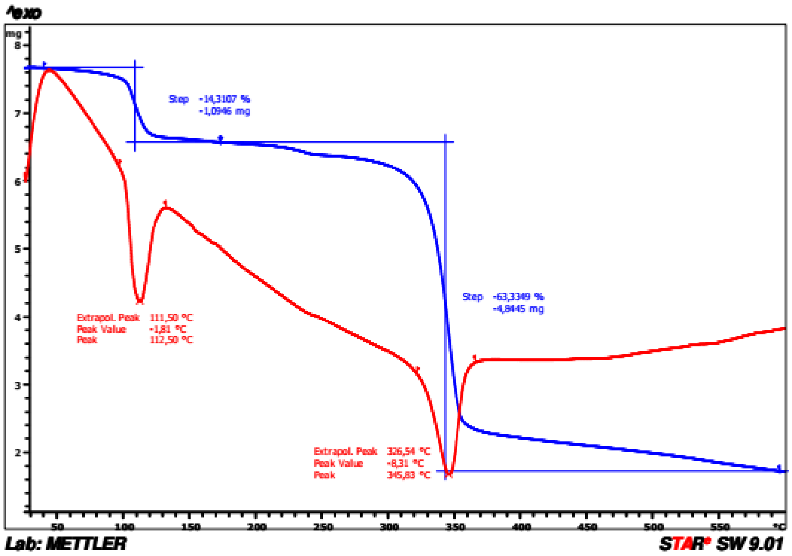

Figure S6.1. Thermal decomposition curve for **1**.

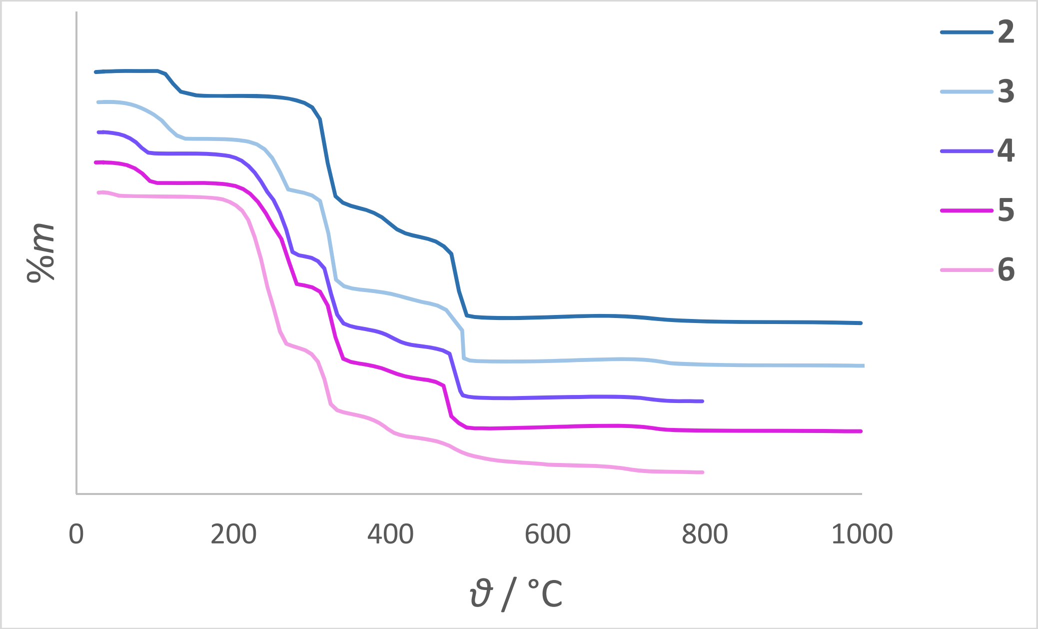

Figure S6.2. Thermal decomposition curves for compounds **2**–**6**.

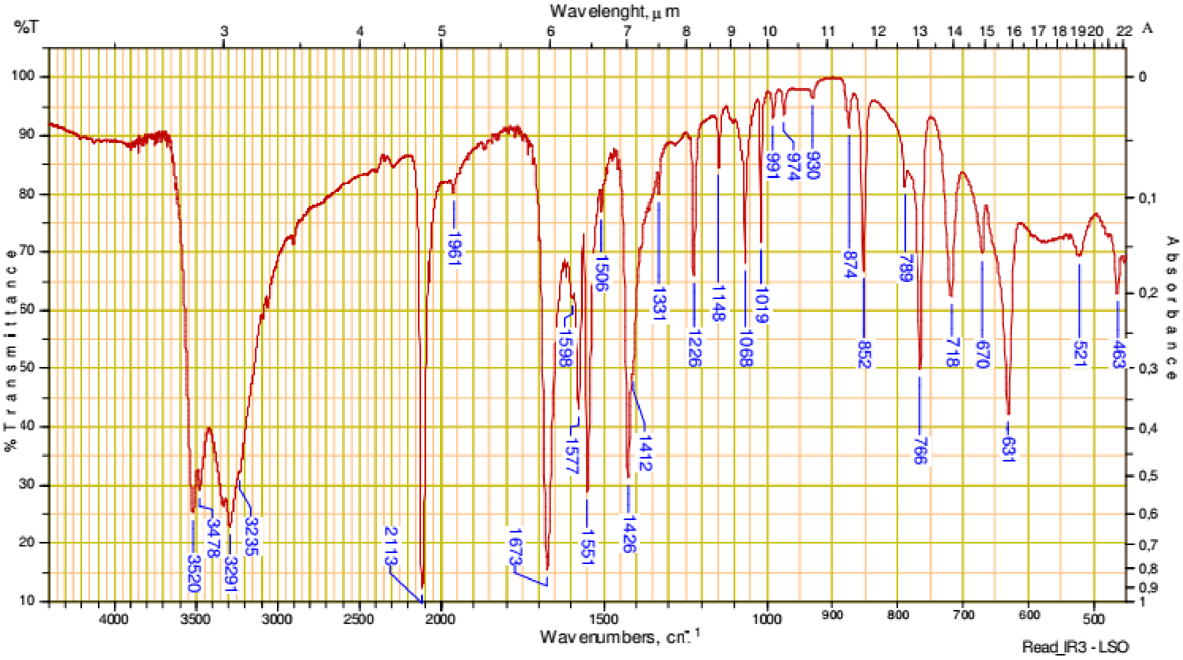

Figure S7.1. IR spectrum of [Ni(NCS)$_2$(isn)$_2$(H$_2$O)$_2$]·2H$_2$O (**1**).

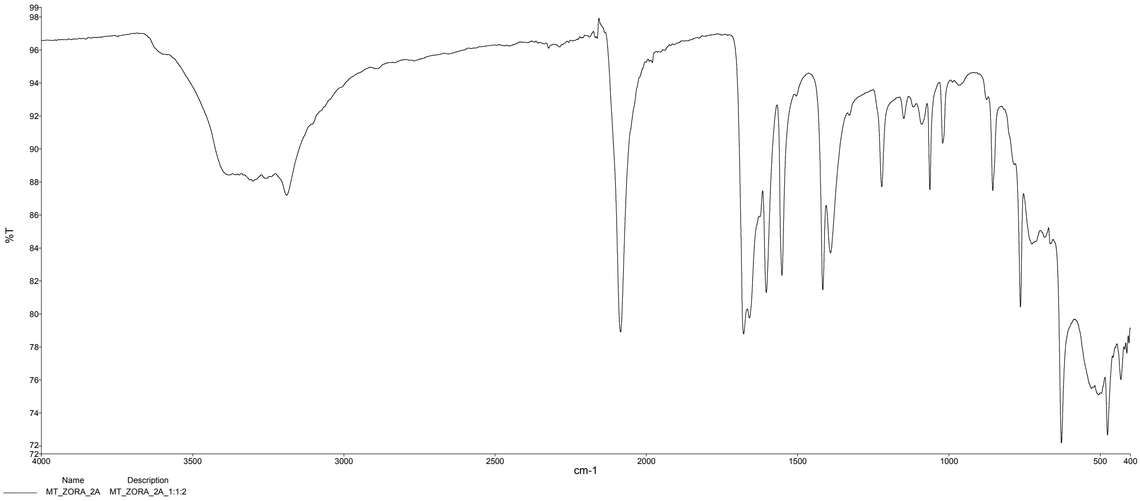

X (cm^{-1})	**Y (%T)**
3190.01	87.2
2085.34	78.9
1678.51	78.78
1603.49	81.29
1551.66	82.34
1416.77	81.46
1391.43	83.7
1221.74	87.72
1062.56	87.54
1019.98	90.35
854.56	87.49
762.96	80.42
627.43	72.17
475.18	72.66
431.02	76.02

Figure S7.2. IR spectrum of [Ni(NCS)$_2$(isn)$_2$(H$_2$O)$_2$] (**2**).

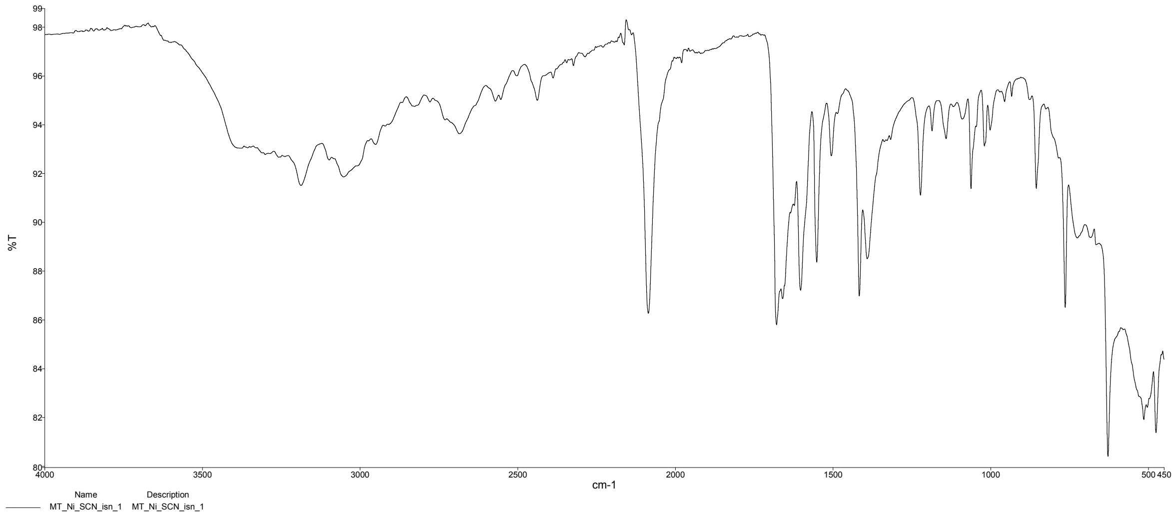

X (cm^{-1})	**Y (%T)**
3188.31	91.52
2085.93	86.27
1679.18	85.8
1602.92	87.22
1551.62	88.37
1505.66	92.73
1416.69	86.98
1391.71	88.51
1222.67	91.12
1062.21	91.39
1019.82	93.13
854.96	91.39
763.17	86.51
627.62	80.4
513.94	81.91
475.29	81.37

Figure S7.3. IR spectrum of $[Ni(NCS)_2(isn)_3(H_2O)]\cdot 2.5H_2O$ (**3**).

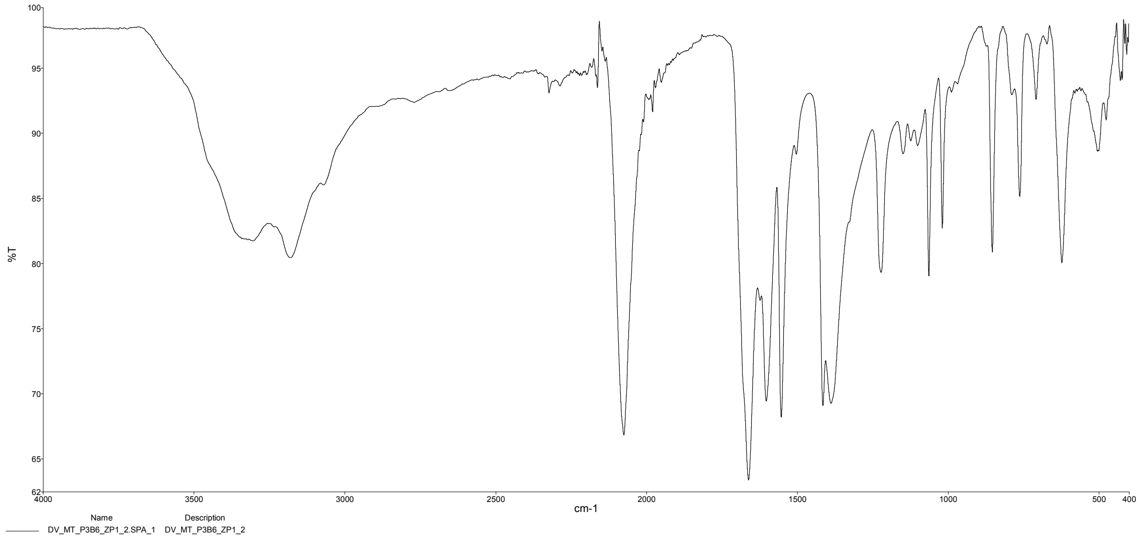

X (cm^{-1})	Y (%T)
3308.5	81.7
3183.01	80.5
2075.0	67.0
1662.4	63.4
1602.9	69.5
1553.7	68.4
1414.1	69.1
1387.4	69.3
1221.2	79.3
1063.1	79.2
1018.0	82.7
853.8	81.1
763.5	85.1
621.8	80.2
502.8	88.6
476.1	91.03
426.9	94.1

Figure S7.4. IR spectrum of $[Ni(NCS)_2(isn)_3(H_2O)]\cdot 3[Ni(NCS)_2(isn)_4]\cdot 9H_2O$ (**4**).

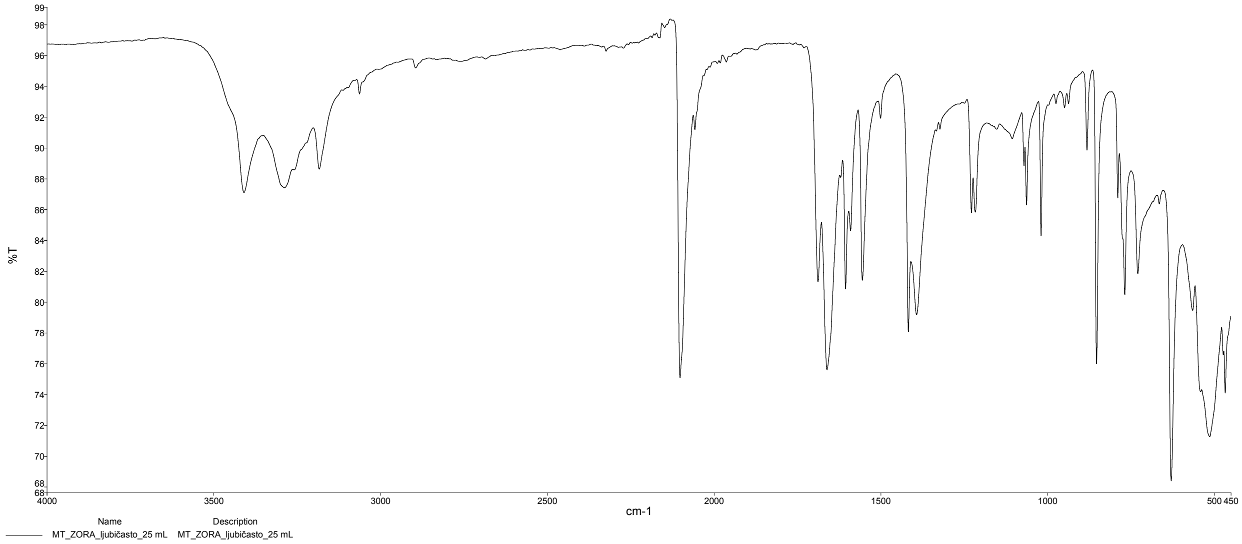

X (cm^{-1})	Y (%T)
3410.15	87.12
3288.89	87.43
3184.5	88.64
2102.01	75.08
1688.34	81.32
1661.38	75.6
1605.55	80.85
1555.07	81.42
1417.18	78.07
1392.49	79.18
1227.92	85.81
1216.34	85.85
1062.66	86.31
1018.97	84.31
881.27	89.88
852.64	76
789	86.78
768.05	80.48
728.78	81.84
628.77	68.38
513.08	71.25
466.64	74.09

Figure S7.5. IR spectrum of $[Ni(NCS)_2(isn)_4]\cdot 3H_2O$ (**5**).

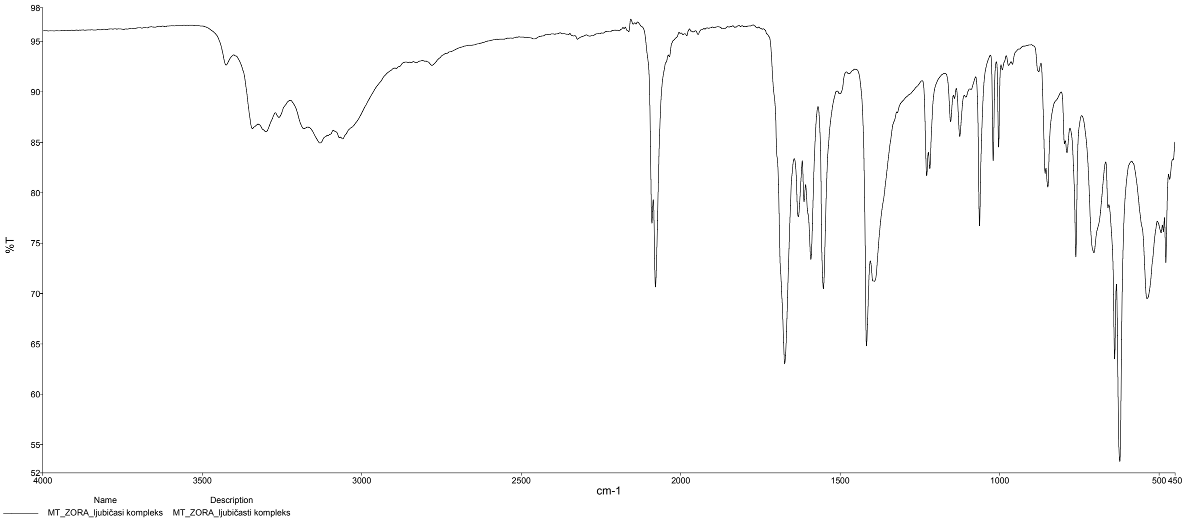

X (cm^{-1})	Y (%T)
3301.00	86.06
3131.53	84.94
2090.17	76.98
2078.96	70.64
1673.73	63.03
1630.88	77.63
1612.85	79.12
1591.57	73.4
1552.26	70.49
1416.99	64.8
1392.33	71.2
1228.26	81.68
1153.28	87.07
1124.55	85.6
1062.62	76.71
1019.62	83.2
1002.62	84.54
848.19	80.56
788.23	83.98
760.42	73.62
703.76	74.05
638.78	63.51
622.49	53.3
536.97	69.51
478.03	73.08

Figure S7.6. IR spectrum of [Ni(NCS)$_2$(isn)$_4$]·2(isn) (**6**).

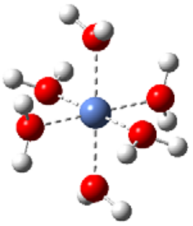

[Ni(H_2O)$_6$]$^{2+}$

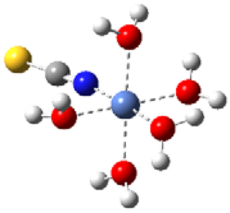

[Ni(H_2O)$_5$(NCS)]$^+$

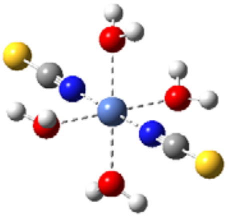

[Ni(H_2O)$_4$(NCS)$_2$]

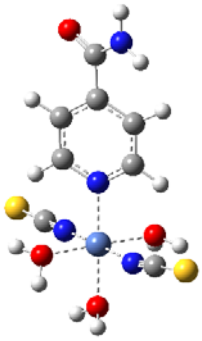

[Ni(H_2O)$_3$(NCS)$_2$(isn)]

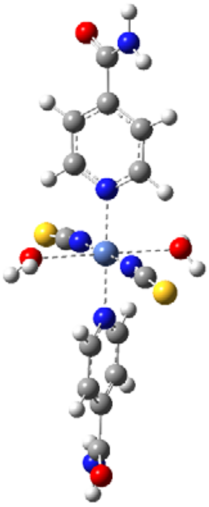

[Ni(H_2O)$_2$(NCS)$_2$(isn)$_2$]

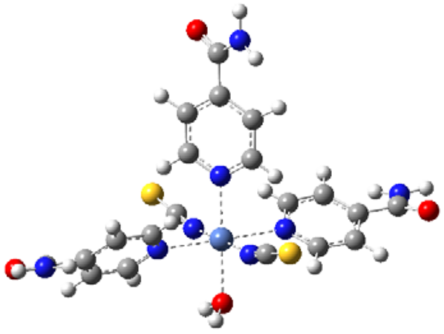

[Ni(H_2O)(NCS)$_2$(isn)$_3$]

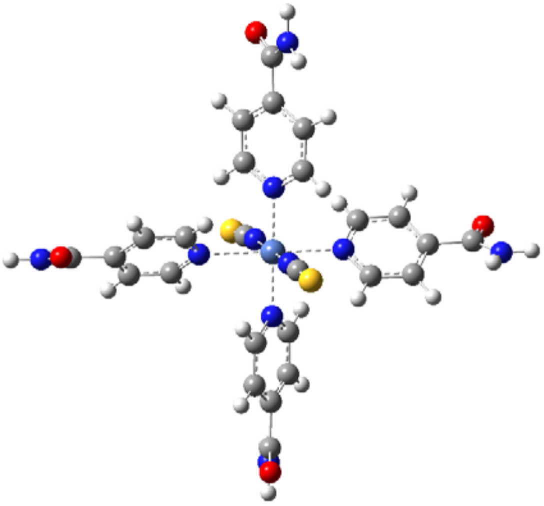

[Ni(NCS)$_2$(isn)$_4$]

Figure S8. Structures of the most stable Ni(II) complexes studied in this work as obtained at the (SMD)/ωB97X–D/LANL2DZ level of theory.

Discussion S3. Computational evaluation of the intermolecular interactions.

In addition to DFT calculations that helped us to explain the formation process of discrete monomers in the aqueous solution, we performed a Hirshfeld surface analysis to study the intermolecular interactions that brought about the isolated crystal complexes. In order to estimate the propensity of two chemical species to be in a contact, we employed CrystalExplorer 21.5 software[S1] that allowed us to generate a set of 2D fingerprints plots (Figures S9–S17) and calculate the enrichment ratios (*E*) of the matching contacts (Tables S7–S9)[S2].

If we compare the established interactions among $[Ni(NCS)_2(isn)_2(H_2O)_2]$ or $[Ni(NCS)_2(isn)_3(H_2O)]$ monomers and solvent molecules, we can get a better insight into the 3D structure of ternary heteroleptic complexes **1**, **2** and **3** (Table S7). All three complexes exhibit highly favoured H···N, H···O and H···S contacts since the matching *E* ratios are higher than unity. These contacts correspond to numerous hydrogen bonds formed between H_2O2···H_2O1/O11/S1, H_2O1···O11 and N12···S1 in **1**, H_2O1/N12···O11/S1 in **2**, and H_2O1···O21, H_2O2···O11, H_2O3···O11/O31, H_2O4···N2/N31, N12/N22/N32···O31/S1/S2 in **3**. In contrast to **2** and **3** where amide nitrogens participate in strong hydrogen bonds with highly electronegative acceptors (E_{HN}=1.59 and 1.42, respectively), in **1** we can observe a decrease in N···H contacts since these groups form only a smaller number of weaker hydrogen bonds with thiocyanate S1 (E_{HN}=0.83) leading to an increased enrichment of C···N interactions as nitrogen becomes more abundant on the molecular surface (E_{CN}=1.73). Remarkable augmentation of C···C contacts in **2** (E_{CC}=3.04) and **3** (E_{CC}=2.03) can be explained by the presence of face-to-face π-stacking interactions, while in complex **1** the uncoordinated water molecule is engaged in the formation of hydrogen bonds in such a way that layered arrangements of pyridine rings are prevented and only T-shaped π-stacking is possible which increases the E_{HC} enrichment (1.26), but impoverishes E_{CC} (0.65). The enrichments ratios of S contacts confirm the propensity of sulphur atom to form chalcogen bonds between C-S1 and N12 in **1** (E_{NS}=1.00) and C-S1···O31 in **3** (E_{OS}=1.04), while no such interactions were detected in **2**.

A complex structure of the crystal **4** is characterized by numerous hydrogen bonds formed between discrete monomers inside the unit cell, like head-to-head amide-amide (N42···O121, O41···N122) hydrogen bonds, as well as those between two different monomers, such as N142···O141, O141···N142 or N122···O91. The uncoordinated co-crystallized water molecules play an important role in construction of the final 3D composition by binding to oxygen (H_2O1···O121, H_2O2··· H_2O1, H_2O4···O121, H_2O9···O101), nitrogen (H_2O6···N82, H_2O7···N152, H_2O9···N142, H_2O10···N62) and sulphur (H_2O2/H_2O10···S5, H_2O3···S1, H_2O6···S7, H_2O7···S3, H_2O8···S8) atoms. All of these interactions resulted in enrichment ratios E_{HN}, E_{HO} and E_{HS} higher than unity (Table S8). It can be observed that C···C contacts are highly enriched (E_{CC}>1), which can be explained by the presence of π···π stacking interactions. Aromatic pyridine rings are also involved in the sulphur···π and oxygen···π bonding which favour C···S/O contacts on the molecular surface (E_{CS} and E_{CO}>1).

Complexes **6** and **7** feature highly favoured H···N, H···O and H···S contacts with the computed enrichment ratios greater than 1 (Table S9). In **7** these interactions originate from hydrogen bonds formed between co-crystallized waters and isn/SCN components: H_2O1···N12/S1/S2, H_2O2···N42/O71, H_2O3···N62, as well as among coordinated ligands of different monomers: N22···O41, N72···O21, N32···O11, N82···O31, N22···S4, N52···S3. They are even more preferred in **6** where the carboxamide groups are arranged in chains among different monomers (O21=C-N22H_2···O31=C-N32H_2) and also act as hydrogen bond donors to the sulphur (N42···S1) and the pyridine nitrogen of the free isn ligand. Relative to **7**, an increase of the E_{HS} enrichment ratio in **6** is also contributed by weak, but not negligible hydrogen bonds of the C-H···S type. Although π-stacking interactions are established in **7**, uncoordinated isn molecules in **6** participate in the face-to-face π-stacking with each other and with aromatic rings from coordinated ligands which is reflected in the increase of C···C contacts (E_{CC}=1.86 and E_{CC}=1.68). Contrary to that, C···S contacts as a result of the sulphur···π bonding are more favoured in **7** than in **6** which is why the enrichment ratio is remarkably increased (E_{CS}=2.15 and E_{CS}=1.76).

In order to ascertain how the electronic structure affects the crystal formation, we have performed a series of quantum-chemical computations aimed at identification of the most positive and negative parts of the monomers $[Ni(NCS)_2(isn)_2(H_2O)_2]$, $[Ni(NCS)_2(isn)_3(H_2O)]$ and $[Ni(NCS)_2(isn)_4]$ (Figure S18). In all discrete units the same groups behave in a similar way, so we can observe that the most negative electrostatic potential (ESP) values correspond to the amide oxygen, while the most positive areas are found on the NH_2 hydrogen atoms. This provides the amide groups with the possibility to participate in the formation of hydrogen bonds that were detected in all of the isolated complexes. The hydrogen atoms of the coordinated water molecules show positive values comparable to those of the amide group as a result of the interaction with the Ni^{2+} metal centre that significantly increases their acidity. It is interesting to notice that the most negative ESP value is not located on the NCS^- anion since its negative charge is resonantly dispersed between N and S atoms (Table 3), but the presence of a region with a slightly positive potential in the centre of the molecular surface (σ-hole) allows thiocyanate to form chalcogen bondings of the C-S···N, O or π type, which turned out to be favourable in all complexes (Tables S7–S9).

Table S7. Hirshfeld contact surfaces and thereof derived random contacts (*R*) and enrichment ratios (*E*) for complexes **1**–**3**. Contact values at the top of the table are obtained through the CrystalExplorer 21.5 software.[S1] Enrichment ratios were not computed for random contacts lower than 0.9%, as they are not meaningful according to literature recommendations.[S2]

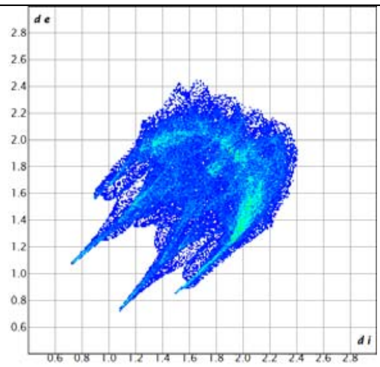

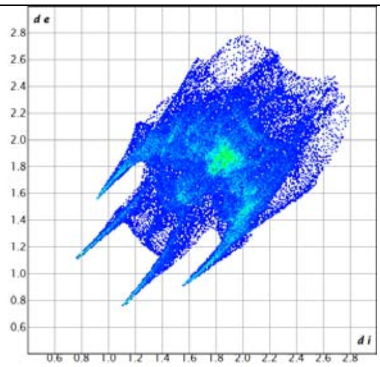

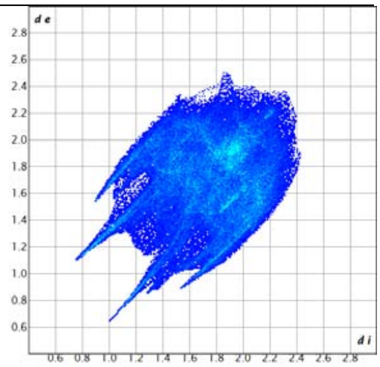

	Complex 1					**Complex 2**					**Complex 3**				
	H	**C**	**N**	**O**	**S**	**H**	**C**	**N**	**O**	**S**	**H**	**C**	**N**	**O**	**S**
Contacts (*C*, %)															
H	23.2	-	-	-	-	24.6	-	-	-	-	27.0	-	-	-	-
C	23.2	1.7	-	-	-	11.0	8.5	-	-	-	17.7	6.5	-	-	-
N	3.3	1.9	0.0	-	-	7.8	0.8	0.0	-	-	5.1	1.0	0.1	-	-
O	19.8	0.7	0.8	0.0	-	16.2	2.3	0.1	0.0	-	17.5	1.7	0.0	0.0	-
S	21.1	3.2	0.9	0.0	0.2	25.3	2.0	0.4	0.7	0.3	18.1	2.4	0.1	2.7	0.0
Surface (*S*, %)															
	56.9	16.2	3.5	10.6	12.8	54.8	16.6	4.5	9.6	14.5	56.2	17.9	3.2	11.0	11.7
Random contacts (*R*, %)															
H	32.4	-	-	-	-	30.0	-	-	-	-	31.6	-	-	-	-
C	18.4	2.6	-	-	-	18.2	2.8	-	-	-	20.1	3.2	-	-	-
N	4.0	1.1	0.1	-	-	4.9	1.5	0.2	-	-	3.6	1.1	0.1	-	-
O	12.1	3.4	0.7	1.1	-	10.5	3.2	0.9	0.9	-	12.4	3.9	0.7	1.2	-
S	14.6	4.1	0.9	2.7	1.6	15.9	4.8	1.3	2.8	2.1	13.2	4.2	0.7	2.6	1.4
Enrichment ratios (*E*)															
H	0.72	-	-	-	-	0.82	-	-	-	-	0.85	-	-	-	-
C	1.26	0.65	-	-	-	0.60	3.04	-	-	-	0.88	2.03	-	-	-
N	0.83	1.73	-	-	-	1.59	0.53	-	-	-	1.42	0.91	-	-	-
O	1.64	0.21	-	0.00	-	1.54	0.72	0.11	0.00	-	1.41	0.44	-	0.00	-
S	1.45	0.78	1.00	0.00	0.13	1.59	0.42	0.31	0.25	0.14	1.37	0.57	-	1.04	0.00

Table S8. Hirshfeld contact surfaces and thereof derived random contacts (*R*) and enrichment ratios (*E*) for four components of the complex **4**. Contact values at the top of the table are obtained through the CrystalExplorer 21.5 software.[S1] Enrichment ratios were not computed for random contacts lower than 0.9%, as they are not meaningful according to literature recommendations.[S2]

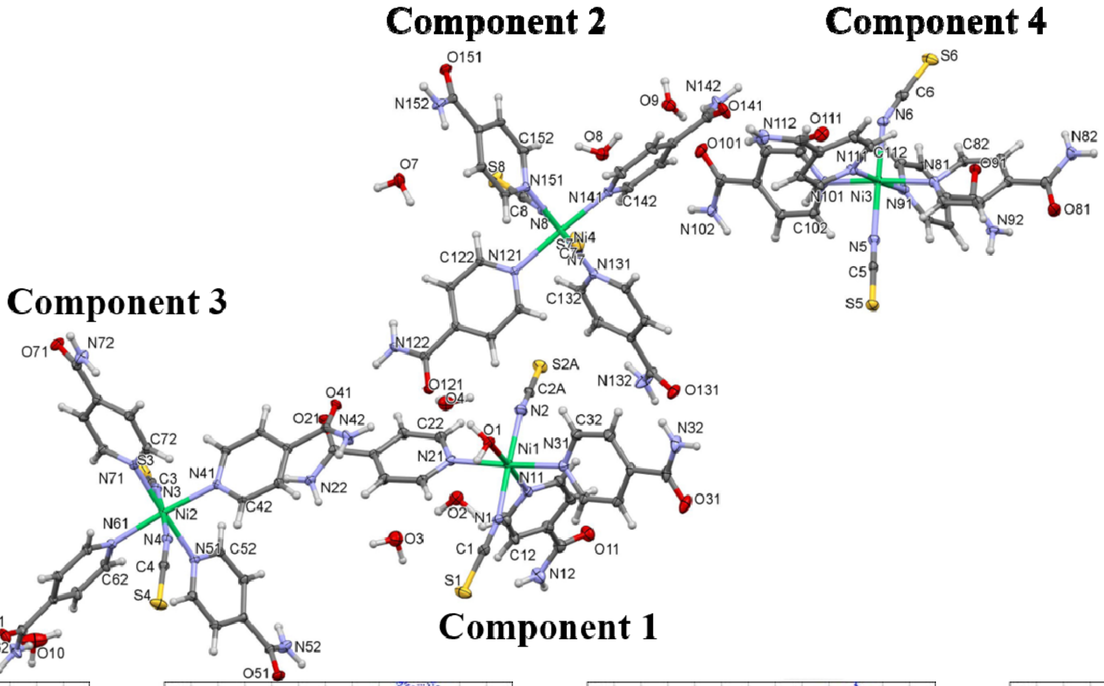

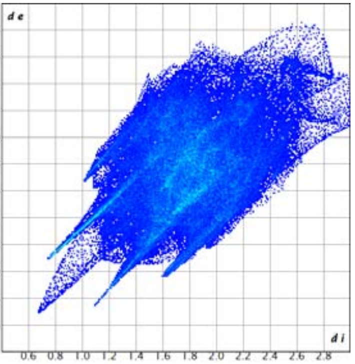

Complex 4_1

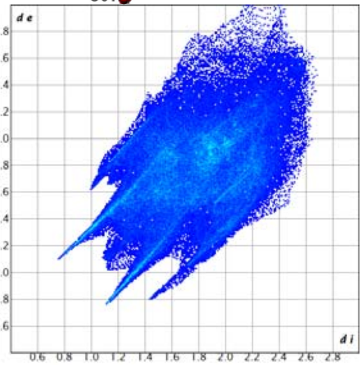

Complex 4_2

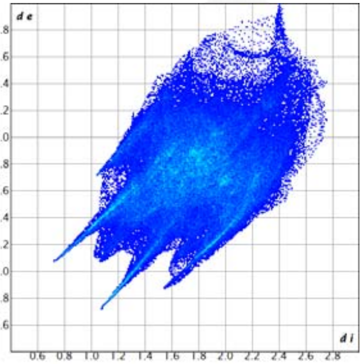

Complex 4_3

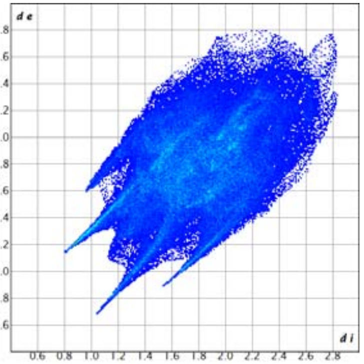

Complex 4_4

	H	**C**	**N**	**O**	**S**	**H**	**C**	**N**	**O**	**S**	**H**	**C**	**N**	**O**	**S**	**H**	**C**	**N**	**O**	**S**
Contacts (*C*, %)																				
H	26.9	-	-	-	-	28.6	-	-	-	-	31.9	-	-	-	-	30.4	-	-	-	-
C	16.1	2.1	-	-	-	15.6	4.0	-	-	-	15.8	2.5	-	-	-	13.1	2.7	-	-	-
N	3.5	0.9	0.1	-	-	2.3	1.7	0.2	-	-	2.5	1.1	0.0	-	-	2.9	1.3	0.2	-	-
O	20.5	2.8	0.1	0.5	-	22.6	2.2	0.0	0.0	-	21.7	4.5	0.2	0.0	-	21.1	3.9	0.0	0.2	-
S	21.6	4.6	0.3	0.0	0.0	17.0	5.1	0.3	0.6	0.0	16.7	2.6	0.2	0.2	0.0	19.2	4.5	0.4	0.0	0.0
Surface (*S*, %)																				
	57.8	14.3	2.5	12.2	13.2	57.3	16.3	2.3	12.7	11.5	60.3	14.5	2.0	13.3	9.9	58.6	14.1	2.5	12.7	12.1
Random contacts (*R*, %)																				
H	33.4	-	-	-	-	32.8	-	-	-	-	36.4	-	-	-	-	34.3	-	-	-	-
C	16.5	2.0	-	-	-	18.7	2.7	-	-	-	17.5	2.1	-	-	-	16.5	2.0	-	-	-
N	2.9	0.7	0.1	-	-	2.6	0.7	0.1	-	-	2.4	0.6	0.0	-	-	2.9	0.7	0.1	-	-
O	14.1	3.5	0.6	1.5	-	14.6	4.1	0.6	1.6	-	16.0	3.9	0.5	1.8	-	14.9	3.6	0.6	1.6	-
S	15.3	3.8	0.7	3.2	1.7	13.2	3.7	0.5	2.9	1.3	11.9	2.9	0.4	2.6	1.0	14.2	3.4	0.6	3.1	1.5
Enrichment ratios (*E*)																				
H	0.81	-	-	-	-	0.87	-	-	-	-	0.88	-	-	-	-	0.89	-	-	-	-
C	0.98	1.05	-	-	-	0.83	1.48	-	-	-	0.90	1.19	-	-	-	0.79	1.35	-	-	-
N	1.21	-	-	-	-	0.88	-	-	-	-	1.04	-	-	-	-	1.00	-	-	-	-
O	1.45	0.80	-	0.33	-	1.55	0.54	-	0.00	-	1.36	1.15	-	0.00	-	1.42	1.08	-	0.13	-
S	1.41	1.21	-	0.00	0.00	1.29	1.38	-	0.21	0.00	1.40	0.90	-	0.08	0.00	1.35	1.32	-	0.00	0.00

Table S9. Hirshfeld contact surfaces and thereof derived random contacts (*R*) and enrichment ratios (*E*) for complexes **6**–**7**. Contacts values at the top of the table are obtained through the CrystalExplorer 21.5 software.[S1] Enrichment ratios were not computed for random contacts lower than 0.9%, as they are not meaningful according to literature recommendations.[S2]

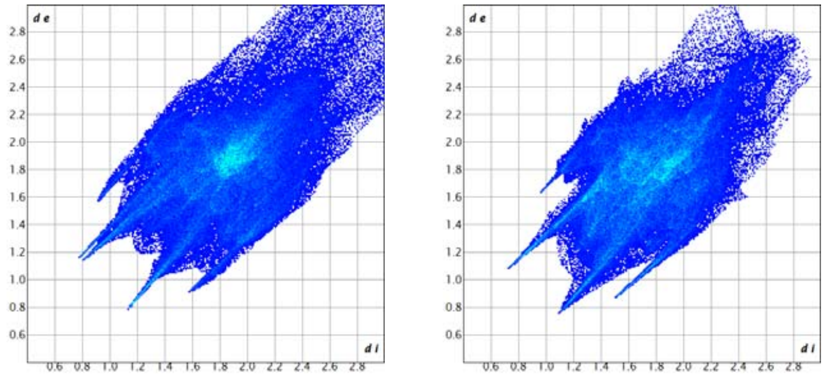

	Complex 6					**Complex 7**				
	H	**C**	**N**	**O**	**S**	**H**	**C**	**N**	**O**	**S**
Contacts (*C*, %)										
H	31.4	-	-	-	-	33.8	-	-	-	-
C	14.1	3.9	-	-	-	11.5	4.2	-	-	-
N	7.0	0.6	0.0	-	-	3.0	0.8	0.0	-	-
O	21.8	1.2	0.2	0.0	-	21.0	3.3	0.1	0.4	-
S	14.0	5.1	0.4	0.3	0.0	13.4	7.3	0.6	0.3	0.1
Surface (*S*, %)										
	59.9	14.4	4.1	11.7	9.9	58.3	15.7	2.3	12.8	10.9
Random contacts (*R*, %)										
H	35.9	-	-	-	-	34.0	-	-	-	-
C	17.3	2.1	-	-	-	18.3	2.5	-	-	-
N	4.9	1.2	0.2	-	-	2.7	0.7	0.1	-	-
O	14.0	3.4	1.0	1.4	-	14.9	4.0	0.6	1.6	-
S	11.9	2.9	0.8	2.3	1.0	12.7	3.4	0.5	2.8	1.2
Enrichment ratios (*E*)										
H	0.87	-	-	-	-	0.99	-	-	-	-
C	0.82	1.86	-	-	-	0.63	1.68	-	-	-
N	1.43	0.50	-	-	-	1.11	-	-	-	-
O	1.56	0.35	0.20	0.00	-	1.41	0.83	-	0.25	-
S	1.18	1.76	-	0.13	0.00	1.06	2.15	-	0.11	0.08

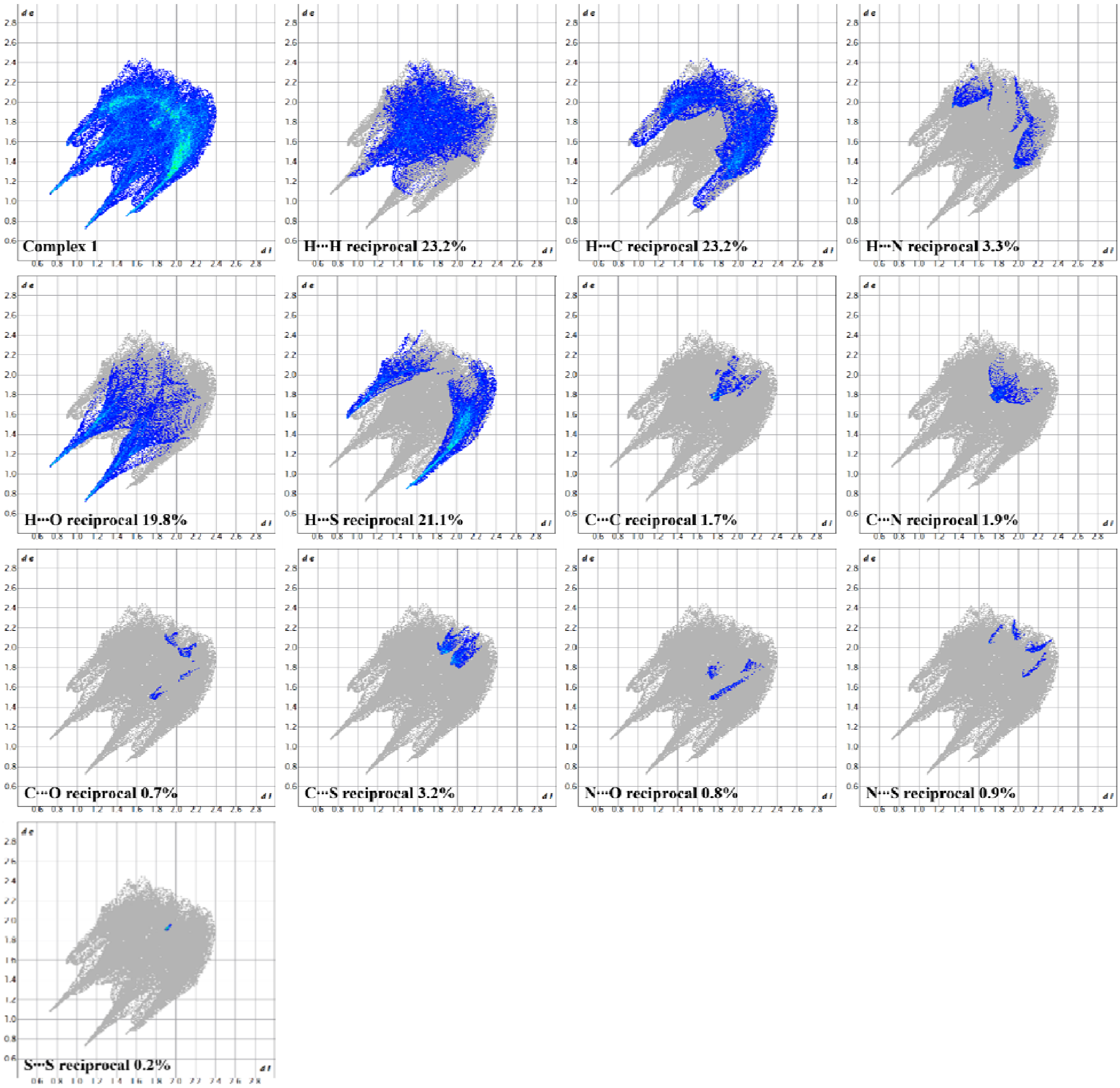

Figure S9. 2D and decomposed 2D fingerprint plots of observed contacts in **1**.

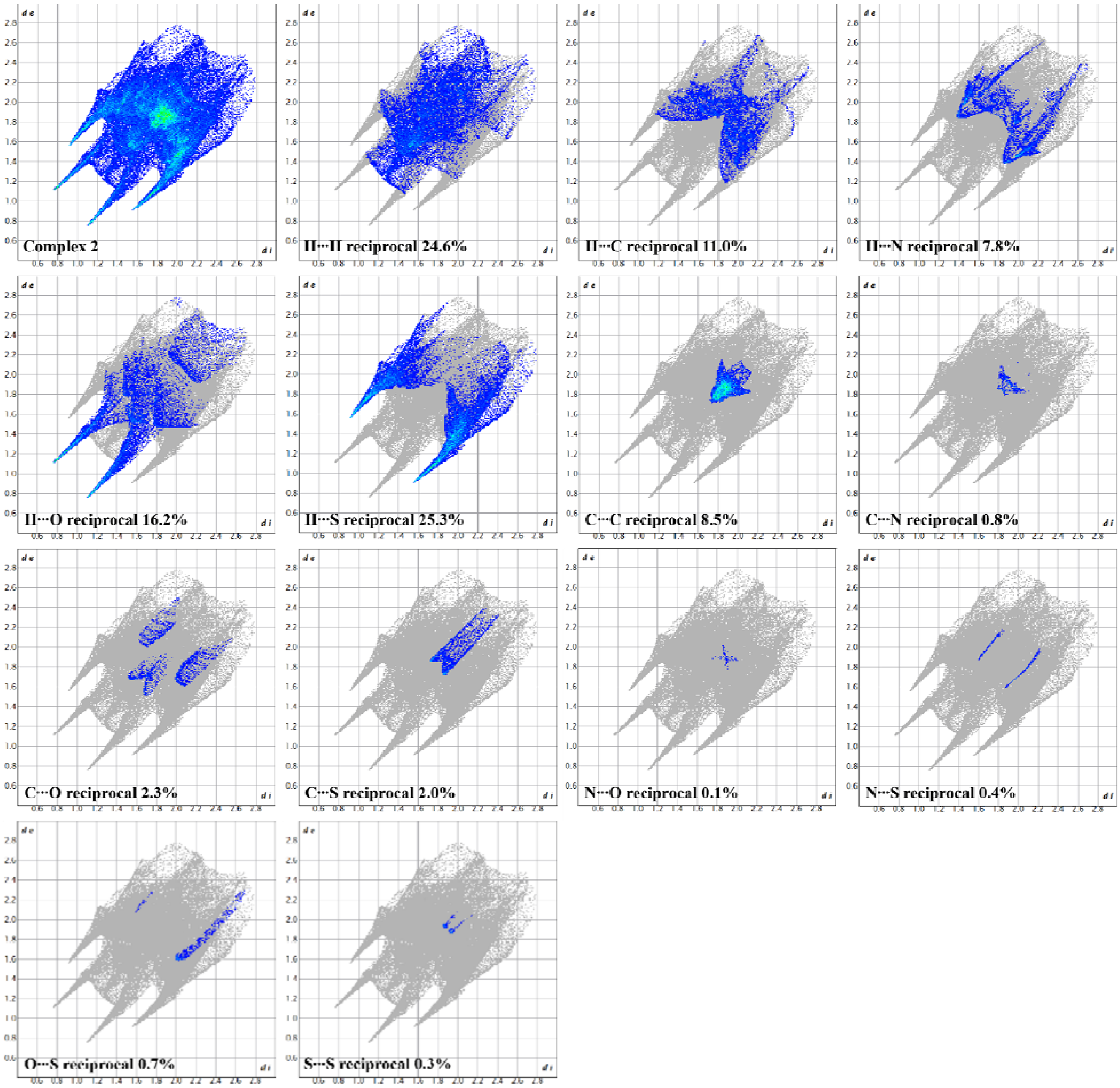

Figure S10. 2D and decomposed 2D fingerprint plots of observed contacts in **2**.

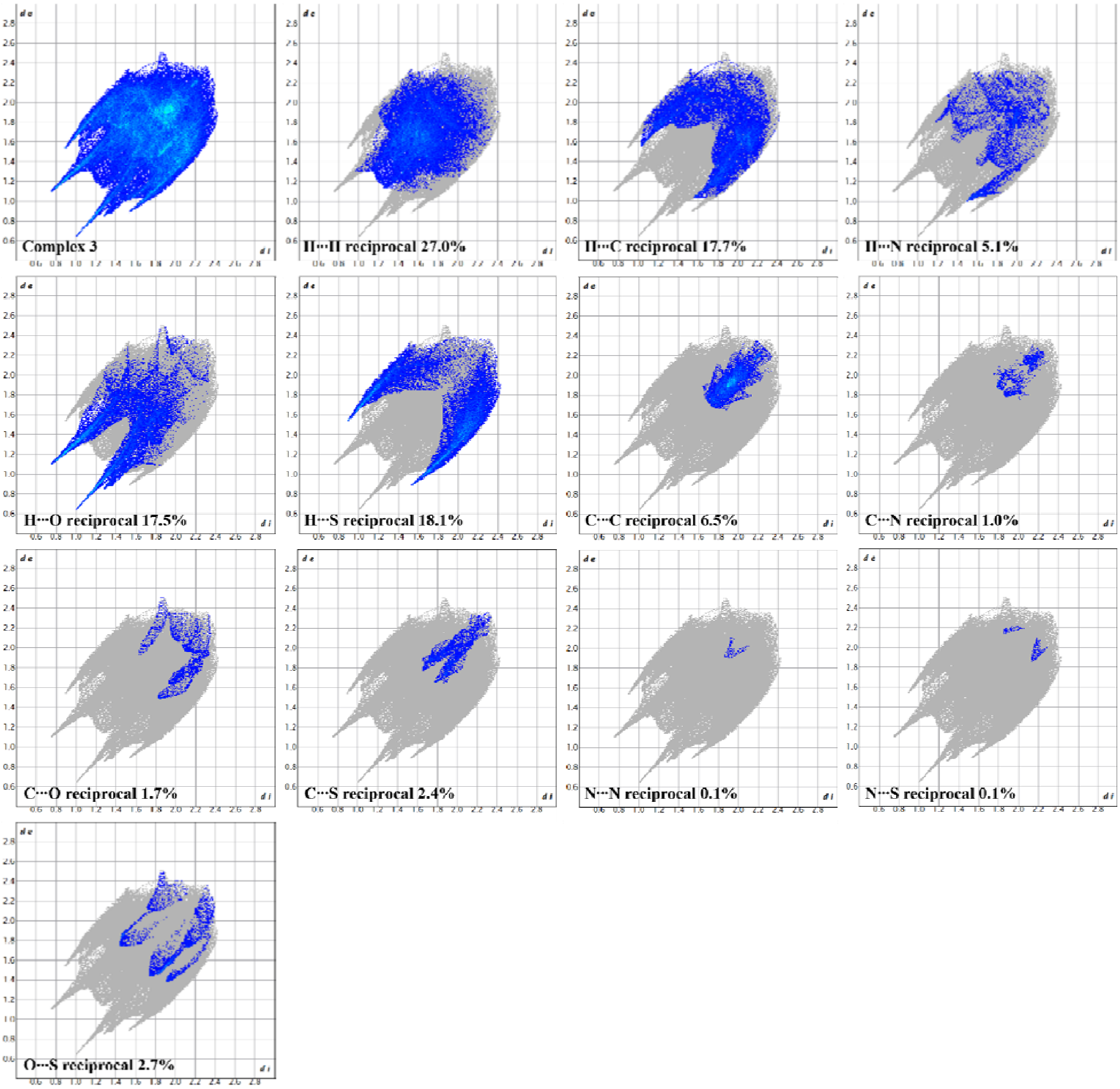

Figure S11. 2D and decomposed 2D fingerprint plots of observed contacts in **3**.

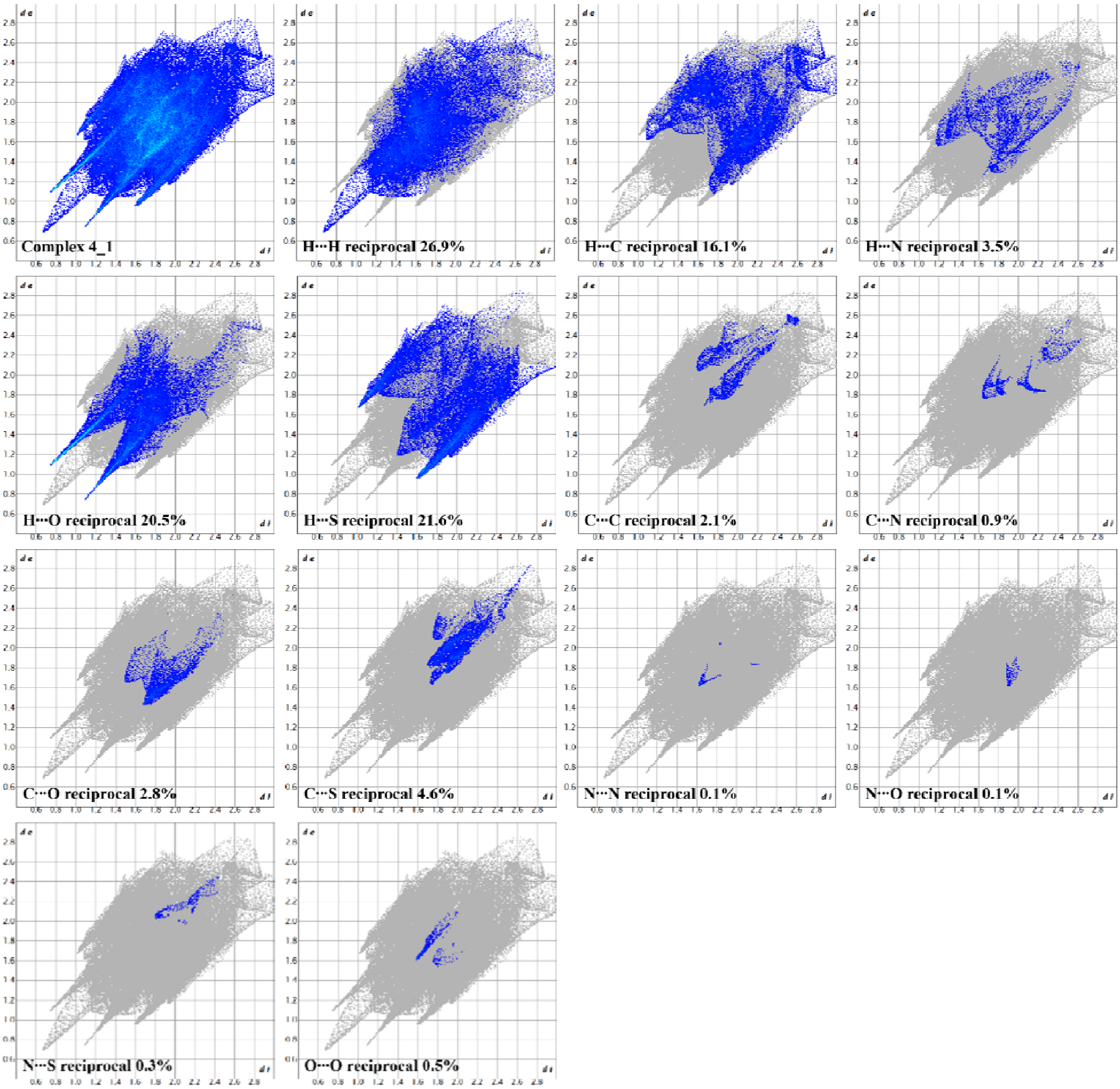

Figure S12. 2D and decomposed 2D fingerprint plots of observed contacts for the first component in **4**.

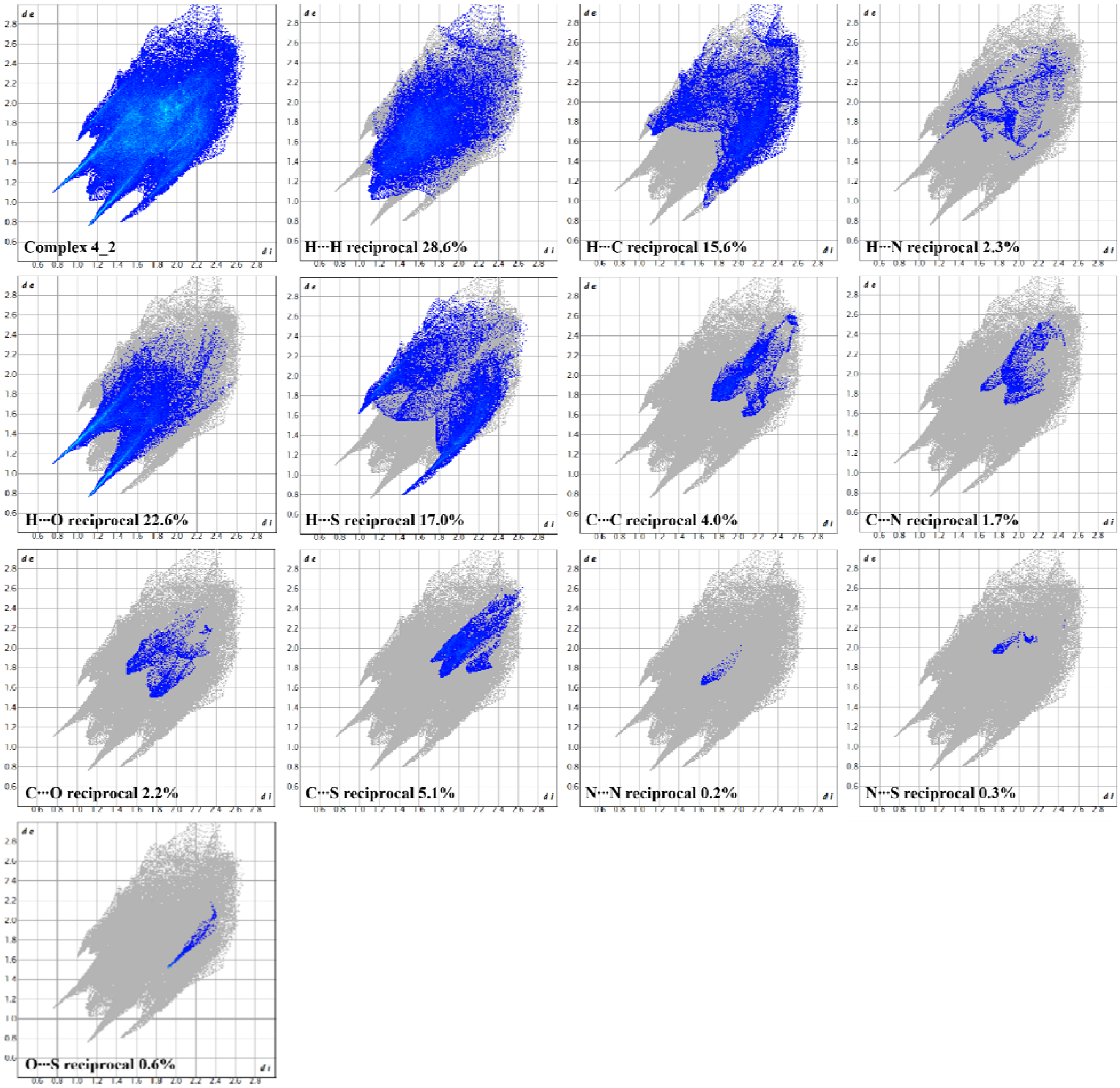

Figure S13. 2D and decomposed 2D fingerprint plots of observed contacts for the second component in **4**.

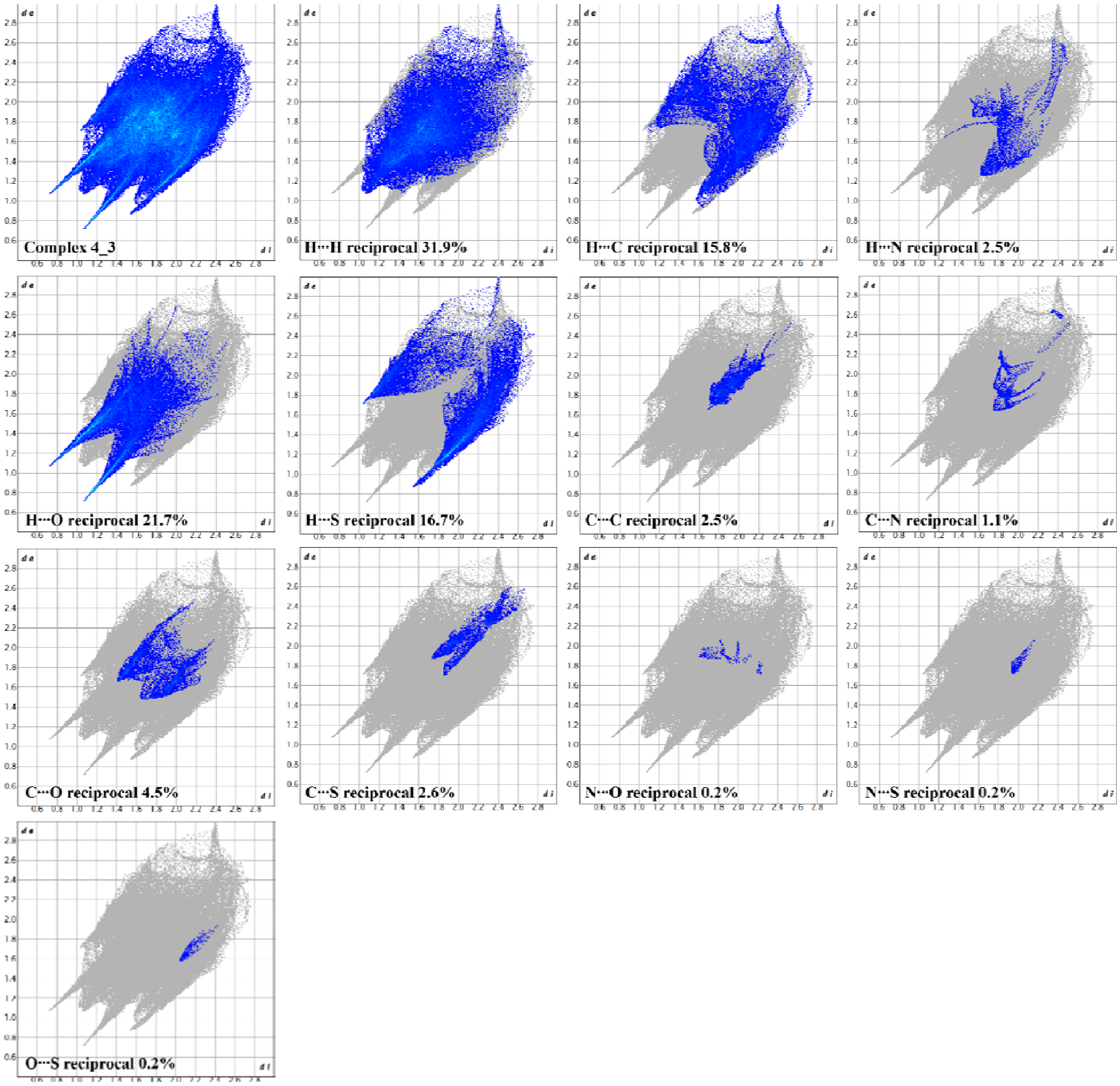

Figure S14. 2D and decomposed 2D fingerprint plots of observed contacts for the third component in **4**.

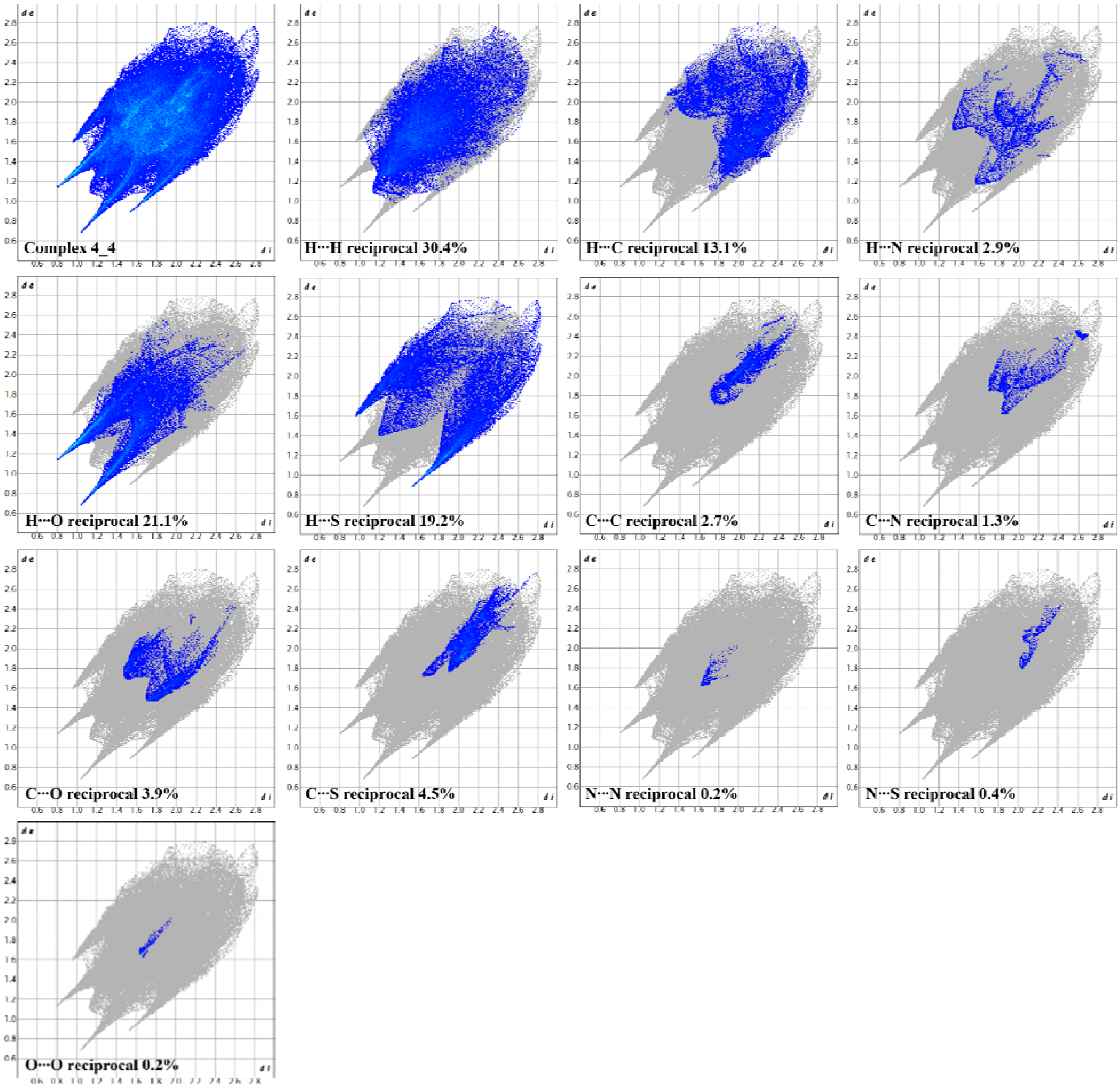

Figure S15. 2D and decomposed 2D fingerprint plots of observed contacts for the fourth component in **4**.

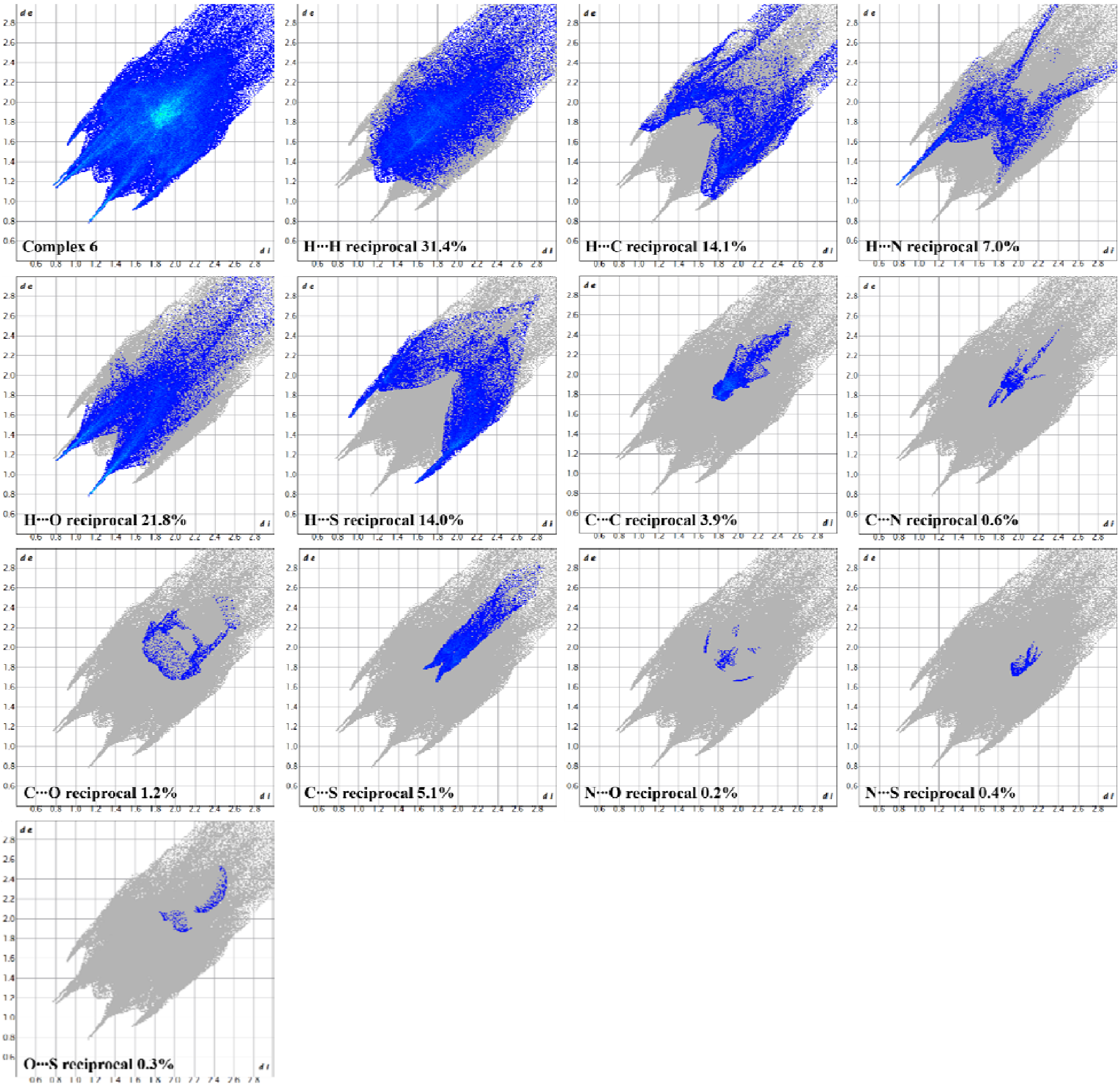

Figure S16. 2D and decomposed 2D fingerprint plots of observed contacts in **6**.

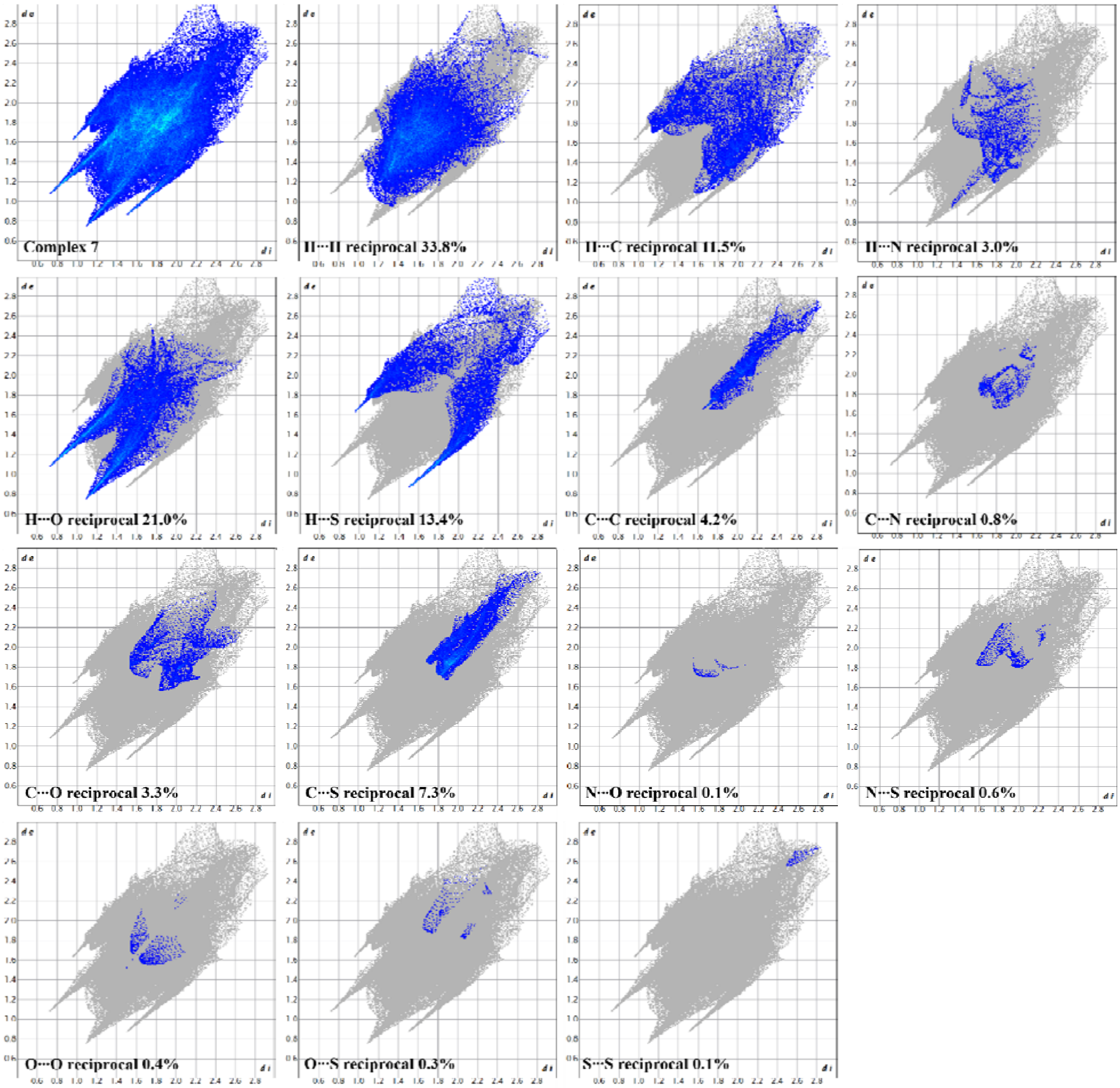

Figure S17. 2D and decomposed 2D fingerprint plots of observed contacts in **7**.

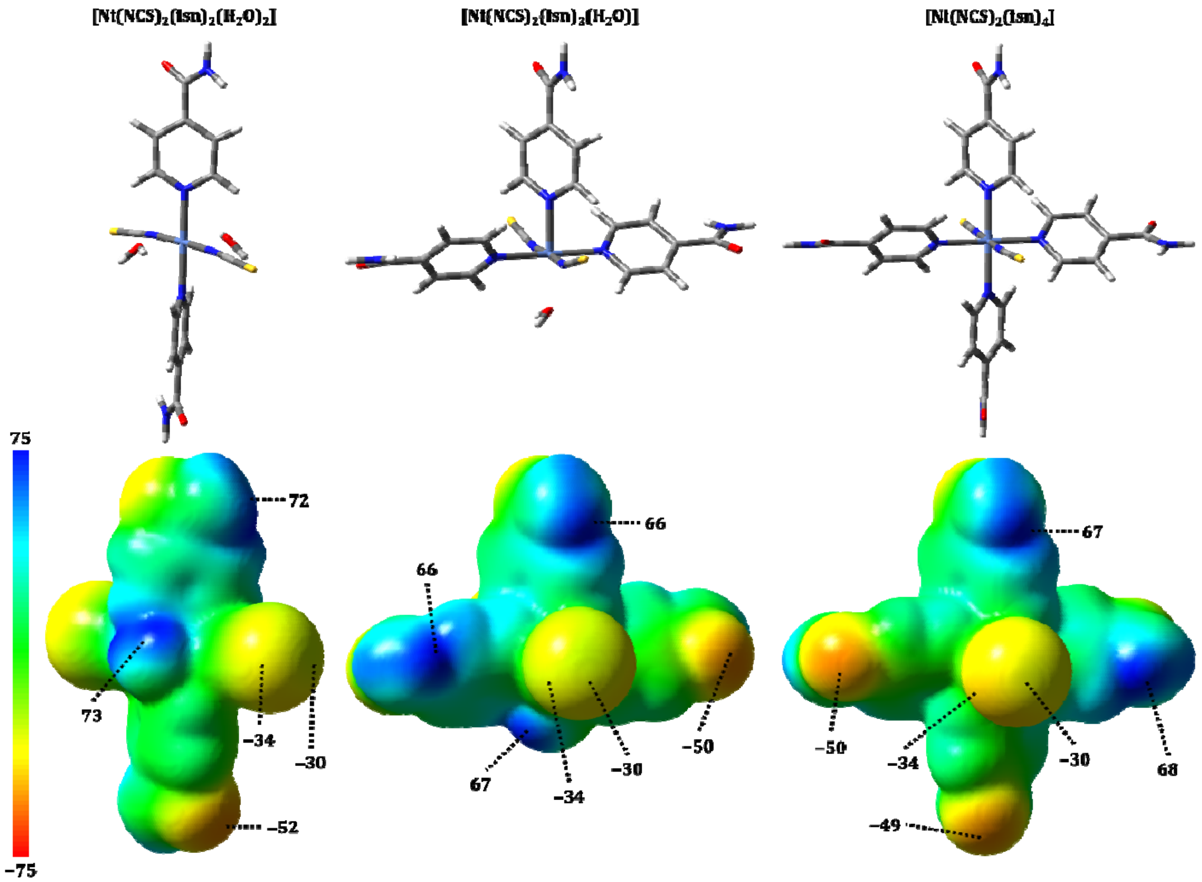

Figure S18. Electrostatic potential (ESP) mapped on the electron density isosurface (ρ_{el} = 0.0004 au) in the monomers [$Ni(NCS)_2(isn)_2(H_2O)_2$], [$Ni(NCS)_2(isn)_3(H_2O)$] and [$Ni(NCS)_2(isn)_4$]. Boundaries of ESP values are given in kcal mol^{-1} e^{-1}.

Supporting Information References

S1 P. R. Spackman, M. J. Turner, J. J. McKinnon, S. K. Wolff, D. J. Grimwood, D. Jayatilaka and M. A. Spackman, *J. Appl. Cryst.*, 2021, **54**, 1006.

S2 C. Jelsch, K. Ejsmont and L. Huder, *IUCrJ*, 2014, **1**, 119.